

TIME VARIATIONS OF THE GEOMAGNETIC FIELD RECORDED IN OCEANIC
SEDIMENTS

By

YOHAN J.B. GUYODO

A DISSERTATION PRESENTED TO THE GRADUATE SCHOOL
OF THE UNIVERSITY OF FLORIDA IN PARTIAL FULFILLMENT
OF THE REQUIREMENTS FOR THE DEGREE OF
DOCTOR OF PHILOSOPHY

UNIVERSITY OF FLORIDA

2002

ACKNOWLEDGMENTS

I am grateful to my advisor, Jim Channell, for the opportunity he gave me to spend a few years in Florida, where I was able to pursue my doctoral research while enjoying the nice weather of the sunshine state. I greatly appreciated his guidance throughout the course of my Ph.D. I also thank the members of my committee, Neil Opdyke, Dave Hodell, Stanley Dermott, and Jean-Pierre Valet, for agreeing to supervise my research during those years. In particular, I greatly appreciated the advice, and the enjoyable collaboration of Jean-Pierre Valet, although mostly accomplished through transatlantic e-mails.

I also had the great pleasure to interact or collaborate with a number of talented people: Gary Acton, Stefanie Brachfeld, Mark Davidson, Kendall Fountain, Philippe Gaillot, Jonathan Glen, Kainian Huang, Laure Meynadier, Albina Mikhailova, Matt Newville, Carl Richter, Joseph Stoner, Ray Thomas, Holger Tostmann, Tim Vaught, Kathy Venz, and many others.

My research was also made possible by the technical and financial support of several organizations including the National Science Foundation (NSF), the JOIDES U.S. Science Support Advisory Committee (USSAC), and the Graduate Student Council. Support was also provided by the Department of Energy (DOE), the Institute for Rock Magnetism (IRM), the French Ministry of Education, the Institut de Physique du Globe de Paris (IPGP), the College of Liberal Arts and Sciences, the Gerson family, and the department of Geological Sciences at the University of Florida.

I thank all of those who gave me their moral support, which sometimes consisted of long hours of extravagance and festivities in the numerous bars and restaurants of Gainesville, Paris, or San Francisco. I thank in particular Lionel Bouchet, Julie Carlut, Isabelle Clairand, Shelley Day, Helen Evans, Kendall Fountain, Susan Kulp, Christian George, Monika Lipinski, Victoria Mejia, Mike Rosenmeier, Howie Scher, Tom Sievers, Lauren Smith, and Stathis Vissokalis. I express my deepest gratitude to France Lagroix for tolerating me, and brightening my days.

Finally, I would not have been able to accomplish this work without the moral, and sometimes financial, support of my family. I thank my grandmother, Avoie, my mother, Marguerite, and my brother and sister, Yvan and Katia.

TABLE OF CONTENTS

	<u>page</u>
ACKNOWLEDGMENTS	ii
ABSTRACT	vi
INTRODUCTION	1
A SEDIMENTARY PALEOMAGNETIC RECORD OF THE MATUYAMA CHRON FROM THE WESTERN ANTARCTIC MARGIN (ODP SITE 1101).....	7
Introduction.....	7
Geological Setting and Lithology	8
Magnetic Mineralogy and Grain Size	11
Magnetostratigraphy.....	13
Time Scale	16
Relative Paleointensity	17
Comparison with Other Paleointensity Records	21
Conclusions.....	27
WAVELET ANALYSIS OF RELATIVE GEOMAGNETIC PALEOINTENSITY AT ODP SITE 983	29
Introduction.....	29
Spectral Analysis.....	32
Global Power Spectrum.....	32
Evolutionary Power Spectrum	34
Wavelet Analysis	36
Description of the Method	36
Wavelet Power Spectrum of ODP Site 983 Paleointensity Record	41
Cross-Wavelet Spectra	44
Conclusion	47

EFFECTS OF VARIABLE SEDIMENTATION RATES AND AGE ERRORS ON THE RESOLUTION OF SEDIMENTARY PALEOINTENSITY RECORDS..... 52

Introduction.....	52
Construction of the Model.....	54
Variable Sedimentation Rates.....	54
Post-Deposition Remanence Acquisition.....	56
Different Age Models.....	60
Comparison with Real Data.....	62
Results.....	65
Individual Records.....	65
Individual Power Spectra.....	69
Stacking the Records.....	70
Conclusion.....	77

DECONVOLUTION OF U-CHANNEL PALEOMAGNETIC DATA NEAR GEOMAGNETIC REVERSALS AND SHORT EVENTS..... 81

Introduction.....	81
Response Functions.....	83
Deconvolution of U-channels and Comparison with Discrete Samples.....	85
The Bjorn Geomagnetic Event at ODP Sites 983 and 984.....	88
Summary.....	91

CONCLUSIONS AND PERSPECTIVES 94

LIST OF REFERENCES 106

BIOGRAPHICAL SKETCH..... 114

Abstract of Dissertation Presented to the Graduate School
of the University of Florida in Partial Fulfillment of the
Requirements for the Degree of Doctor of Philosophy

TIME VARIATIONS OF THE GEOMAGNETIC FIELD RECORDED IN OCEANIC
SEDIMENTS

By

Yohan J.B. Guyodo

May 2002

Chairman: Dr. James E.T. Channell
Major Department: Geological Sciences

This dissertation addresses the resolution and reliability of paleomagnetic records obtained from oceanic and marine sediments, with a particular focus on records of relative geomagnetic paleointensity. It shows the methods used to recover such signals by constructing a high-resolution paleomagnetic record from the Ocean Drilling Program (ODP) Site 1101, which covers the interval 0.7-2.1 Ma. The reliability of individual paleointensity records can be further tested with time series analysis techniques such as wavelets. This point is illustrated by a spectral analysis of a record of relative geomagnetic paleointensity from ODP Site 983, covering the time interval 0-1.1 Ma. The use of wavelets made it possible to demarcate the intervals over which Earth's orbital frequencies are present in the record. Results of this investigation suggest that the orbital frequencies embedded in the paleointensity record are the expression of lithologic variations, although they have a minor effect on the record.

Variable sedimentation rates and dating errors influence the resolution of paleointensity records. This can be investigated by generating synthetic records of relative paleointensity with a numerical model simulating the recording process in sediments. Also, improvement of the resolution of paleomagnetic records can be achieved by reducing the bias induced by measurement techniques, and in particular the spatial smoothing of u-channel data introduced by the response function of cryogenic magnetometers. For that purpose, the deconvolution scheme developed by Oda and Shibuya has been adapted for the treatment of u-channel data. This program was tested with two u-channels, which showed that large amplitude changes unveiled by the deconvolution treatment are in good agreement with the results obtained on discrete samples extracted from the same u-channels.

All of these methods are essential to the study of geomagnetic variations recorded in marine sediments. However, a full understanding of the complex nature of the magnetization process can only be achieved through a collaborative effort between paleomagnetic, rock-magnetic, and analytical techniques. This should include the use of techniques such as optical and electron microscopy, atomic force microscopy, and novel and sensitive methods such as those related to coherent x-rays generated by synchrotrons.

CHAPTER 1 INTRODUCTION

The Earth's magnetic field, which originates for the main part from the Earth's core, can be described mathematically in term of spherical harmonics (Gauss, 1838), with the first degree (the dipole) representing ~90% of the field. Statistical analyses of the geomagnetic field generally assume the spherical harmonic components to be independent, random gaussian variables with known means, variances, and correlation times (Constable and Parker 1988; Hongre et al. 1998; Hulot and Le Mouel 1994). When compared with historical and archeological data, these statistical models indicate correlation times for terms of Degree 2 or higher that are less than 150 years, while those of the equatorial and axial dipoles are 500 years and much longer, respectively (see review in Dormy et al. 2000). As a consequence, when the field is averaged over a few thousand years, only the variations due to the axial dipole remain, which are global in nature. These changes in the dipole intensity and direction are the ones recorded in marine sediments. The main objective of my doctoral research was to provide an original contribution to the general understanding of past variations of the geomagnetic field recorded in marine sediments. The acquisition of magnetization in marine sediments is a rather complex process, which is not fully understood. At first approximation, the natural remanent magnetization (NRM) of marine sediments originates from the alignment of micron-scale magnetic grains along field lines of the geomagnetic field, soon after deposition of the sediment at the bottom of the ocean. The magnetization is then

progressively locked, as the sediment accumulates and becomes more compact.

Therefore, the direction of the magnetization vector, which is described in terms of inclination and declination (Figure 1-1), reflects the direction of the magnetic field at a time close to the deposition of the sediment.

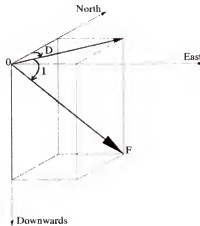


Figure 1-1. Direction of the total vector (F) represented in term of declination (D) and inclination (I). The declination is the angle between the horizontal projection of the total vector and the geographic north, measured eastward. The inclination is the angle between the horizontal plane and the total vector.

The intensity of magnetization is, similarly, proportional to the paleointensity of the magnetic field (or at least the dipole terms). However, it also depends on factors such as relative abundance in magnetic material (linear dependency), or mineralogy and grain size of the magnetic particles (nonlinear dependency). By selecting sediments with homogenous magnetic composition and grain size (using the appropriate magnetic parameters), and by correcting for changes in concentration of the magnetic carriers, it is possible to construct a proxy for the geomagnetic field paleointensity (Review in Tauxe 1993). Commonly used normalizers are low field magnetic susceptibility (χ), and laboratory-induced magnetizations such as the anhysteretic remanent magnetization (ARM) or the isothermal remanent magnetization (IRM). This normalization procedure

provides relative variation in geomagnetic paleointensity (Tauxe 1993). In most cases, because sedimentary processes are often characterized by time constants ranging from hundreds to thousands of years, the magnetic information is averaged in time and only the dipole paleointensity is accessible.

Nevertheless, marine sediments offer the potential of acquiring continuous sequences of geomagnetic paleodirection and relative paleointensity, despite the difficulties inherent to the complexity of the magnetization process (Channell et al. 1997, 1998; Channell and Kleiven 2000; Guyodo et al. 1999, 2001a; Lehman et al. 1996; Meynadier et al. 1992, 1994; Schneider and Mello 1996; Stoner et al. 1995, 2000; Tauxe and Wu 1990; Tauxe and Shackleton 1994; Tric et al. 1992; Valet and Meynadier 1993; Yamazaki et al. 1995). Significant improvements in rock-magnetism, paleomagnetism, and dating techniques have greatly contributed to the acquisition of such detailed records, which display time changes of the field ranging from the small amplitude of the secular variation to major changes such as polarity reversals. An example of such studies is presented in Chapter 2, which addresses paleomagnetic changes recorded in sediments from the western Antarctic margin (Guyodo et al. 2001a).

Other aspects of my research have involved time series analysis of relative paleointensity records. For instance, I established a compilation of 33 records of relative paleointensity from marine sediments documenting the past 800,000 years. On a common time scale, these records have been combined into a synthetic curve defined as Sint-800 (Figure 1-2), and the statistical significance of these results was tested by a bootstrap technique (Guyodo and Valet 1999). One interesting outcome of this study was that, although it is possible to recover global (dipole) paleointensity variations of the

geomagnetic field, there are some discrepancies between individual records, as reflected by the error bars associated with the compilation (Figure 1-2).

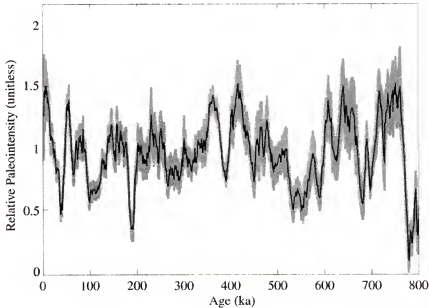


Figure 1-2. Synthetic record of relative paleointensity for the last 800 ky (Sint-800) with its standard error (in grey) obtained from the stack of 33 records of paleointensity. All the records in the compilation have been dated with a common time scale before compilation (Guyodo and Valet 1999).

Some of the differences can be explained in terms of variations in the resolution of the records, alteration of the signal by inappropriate sampling, or because of dating errors. Alternatively, part of the observed discrepancy may be due to the presence of unrecognized, secondary (i.e., nongeomagnetic) signals. This points to limitations in the techniques used to establish individual records and to test their reliability. Some improvement can be achieved by applying time series analysis techniques such as wavelet analysis, which permits an efficient comparison of lithologic and paleomagnetic proxies in the time and frequency domains, therefore allowing recognition, localization, and to some extent quantification of these secondary signals. Using this idea, I performed a wavelet analysis of a record of relative geomagnetic paleointensity from the North

Atlantic Ocean (Guyodo et al. 2000). This study, which is presented in Chapter 3, permitted to describe fundamental aspects of the temporal variability of this record.

I have also developed a model simulating the production of records of relative paleointensity. The resolution and reliability of sedimentary paleointensity records depends strongly on the magnetization process (sedimentation rates, magnetic mineralogy, post-depositional chemical and physical alterations), as well as on the quality of the age model used to date the sediment. One way of testing the reliability of paleointensity records is to develop models simulating magnetization acquisition, paleomagnetic measurements, and dating procedures. I constructed such a model, for which a detailed description is provided in Chapter 4.

In the fifth chapter, I present results from the testing of a numerical code aimed at increasing the resolution of sedimentary paleomagnetic records. High-resolution sedimentary paleomagnetic records are obtained by measuring the natural remanent magnetization of sediment cores using pass-through cryogenic magnetometers, which are equipped with sensors permitting measurement of the sediment magnetization along three axes. The signal provided by the magnetometer is derived from magnetizations lying in the broad region of sensitivity of these sensors. This can be described as a convolution between the response function of the sensor and the actual magnetization of the sample, which results in a smoothing of the original signal. Recently, Oda and Shibuya (1996) developed a numerical code providing the deconvolution of paleomagnetic data obtained from this type of measurements. Their program yielded encouraging results when applied to data obtained on Ocean Drilling Program (ODP) piston cores. The deconvolution scheme developed by Oda and Shibuya (1996) has been implemented at the University of

Florida, for the treatment of paleomagnetic data obtained from the type of samples that are routinely used in the paleomagnetic laboratory. These samples, called u-channels, are transparent plastic tubes ($2 \times 2 \times 150 \text{ cm}^3$) that are used to sample piston cores (Tauxe 1983). Our adapted version of the program has been applied to u-channels from ODP Sites 1090, 983, and 984, which provided interesting results that are reported in Chapter 5.

In the conclusion chapter, I highlight some of my ongoing research on micro- to nanoscale magnetic particles. I have been working on a project aimed at imaging iron-bearing particles such as magnetite (Fe_3O_4), titanomagnetite ($\text{Fe}_{2.4}\text{Ti}_{0.6}\text{O}_4$), hematite ($\alpha\text{-Fe}_2\text{O}_3$), maghemite ($\gamma\text{-Fe}_2\text{O}_3$), goethite ($\alpha\text{-FeOOH}$), and pyrite (FeS_2) in sedimentary rocks. For this purpose, I have been using x-ray techniques available at the Advanced Photon Source (APS) synchrotron at Argonne National Laboratory, along with optical and electron microscopy, to advance our understanding of the genesis, characteristics and evolution of these particles.

CHAPTER 2
A SEDIMENTARY PALEOMAGNETIC RECORD OF THE MATUYAMA CHRON
FROM THE WESTERN ANTARCTIC MARGIN (ODP SITE 1101)

Introduction

Our understanding of the geomagnetic field has increased tremendously—partly because of rapid advances in paleomagnetic techniques and technology, which have facilitated the acquisition of reliable continuous records of relative paleointensity from marine sediments (Channell et al. 1997, 1998; Channell and Kleiven 2000; Guyodo et al. 1999; Meynadier et al. 1992, 1994; Stoner et al. 1995, 2000; Tauxe and Shackleton 1995; Tric et al. 1992; Valet and Meynadier 1993; Yamazaki and Ioka 1995). The growing interest in establishing sedimentary paleointensity records has led to the development of compilations aimed at describing the time evolution of dipole field intensity, as well as providing new stratigraphic correlation tools (Guyodo and Valet 1996, 1999; Laj et al. 2000). Most of the studies that have been published in the past 20 years were limited to low and middle latitudes, with only a few from the high latitudes of the Northern Hemisphere (Channell et al. 1997, 1998, Channell and Kleiven 2000; Laj et al. 2000; Stoner et al. 1998). To establish the global character of the dipole field variations, it is important to obtain paleointensity records from high latitudes in the Southern Hemisphere. The only relative paleointensity records from mid or high latitude Southern Hemisphere are from the subantarctic South Atlantic (Channell et al. 2000). These records can be correlated among several sites, and to records from the Northern

Hemisphere, for the last 100 kyr (Channell et al. 2000; Stoner et al. 2000). More sedimentary paleointensity records from high-latitude sites are needed to understand the long-term evolution of the geodynamo, to study spatial and temporal variations in the strength of the field over periods of constant geomagnetic polarity, and to examine how the field regenerated after polarity reversals (Kok and Tauxe 1996; Mazaud 1996; Meynadier et al. 1994, 1996, 1998; Valet and Meynadier 1993).

In this chapter, I present a geomagnetic record derived from sediments collected on drift deposits off the Western Antarctic Peninsula continental margin, at Ocean Drilling Program Site 1101 (Leg 178). This record provides a magnetostratigraphy down to 2.1 Ma, and a record of relative paleointensity for the period 0.7-1.1 Ma. This high latitude, Southern Hemisphere paleointensity record is aimed at improving the statistical robustness of the database available for this period of time. This chapter was published in the journal *Earth and Planetary Science Letter* (Guyodo et al. 2001a).

Geological Setting and Lithology

Ocean Drilling Program (ODP) Site 1101 (64°22'S, 70°16'W, 3509 m water depth) is located at the crest of a sediment drift on the continental rise of the Antarctic Peninsula Pacific margin (Figure 2-1). This drift is part of a series of eight large hemipelagic sediment drifts (about 130 x 50 x 1 km³ in dimension), which are interpreted to have resulted from the interaction between turbidity currents and bottom currents at the base of the continental slope (Rebesco et al. 1997). The drifts are separated by large channels (up to 5 km wide) formed by turbidity currents that transport sediment from the lower continental slope toward the abyssal plain (Tomlinson et al. 1992). Part of the fine-grained fraction of those turbidity currents is entrained in a bottom current nepheloid

layer. The drifts are constructed above the level of turbidity flow by the down-current deposition of fine-grained suspended material (Rebesco et al. 1997).

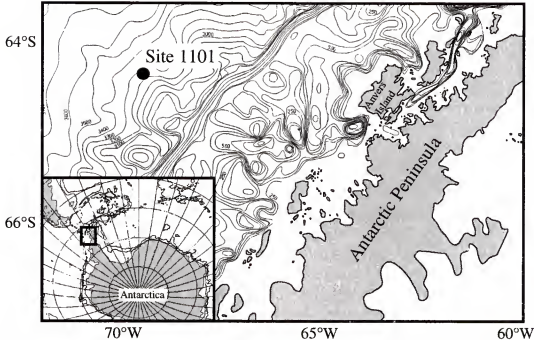


Figure 2-1. Location map for ODP Site 1101, on the Western margin of the Antarctic Peninsula.

During ODP Leg 178, the sediment was collected by advanced piston corer (APC) down to 142.7 mbsf (meters below sea floor), then cored with the extended core barrel (XCB) technique down to 217 mbsf (Shipboard Scientific Party 1999). The recovered sedimentary sequence consisted essentially of hemipelagic clayey silt, and was divided into three lithological units during shipboard analyses (Shipboard Scientific Party 1999). Unit I (0-53 mbsf) comprises alternations of laminated and massive clayey silts that are interpreted as the expression of glacial and interglacial periods, respectively. In this unit, the intervals corresponding to warm periods are indicated by the presence of diatom-bearing layers. Similar alternations were observed in the underlying unit (Unit II, 53-142.7 mbsf), but here the warm intervals are characterized by foraminifera-bearing

layers. The laminated facies of Unit II is characterized by millimeter-thick bioturbated silty clay laminations, which appear as subtle color banding. They suggest a low-energy depositional setting dominated by weak bottom contour currents (Shipboard Scientific Party 1999). As in Unit I, the faint laminations are interpreted as resulting from deposition of the fine-grained fraction of the suspended sediment load associated with turbidity currents (Shipboard Scientific Party 1999). The third unit (Unit III, 142.7-217.7 mbsf) does not display the cyclic pattern observed in Units I and II, and is mostly composed of massive clayey silts that probably originated from the deposition of turbidites, and ice rafted debris.

We sampled the depth interval 50-133 mbsf using 5 cm³ cylinders (at ~1 sample per core section) and U-channel samples (shore-based continuous sampling). This depth interval corresponds roughly to lithologic Unit II. Only one APC hole was cored at Site 1101, so that no composite section is available at this site and small parts of the geological record may be missing. In the unit sampled, laminated intervals alternate with massive intervals. These millimeter-scale laminations are subtle variations within a fairly homogenous silty clay or clayey silt unit. The thickness of the laminations is an order of magnitude smaller than the ~4 cm response function of the magnetometer used in this study. Occasionally, sharp-based, 1 to 3 mm silt laminations are present, probably induced by distal low-density turbidity flows. A few thicker layers, ranging from 0.5 to 4 cm in thickness are also present in the sequence at 66, 87.5, 116.7, and 136.8 mbsf. These are associated with high frequency peaks in the shipboard magnetic susceptibility data (Shipboard Scientific Party 1999), and therefore have been omitted from further study. The massive intervals, attributed to warmer periods, are characterized by lower values of

magnetic susceptibility, probably due to biogenic dilution of the terrigenous input (Shipboard Scientific Party 1999).

Magnetic Mineralogy and Grain Size

We measured the hysteresis properties and low-temperature demagnetization of the discrete samples at the Institute for Rock Magnetism at the University of Minnesota. The hysteresis parameters were measured on a Princeton Measurements Corporation micro-VSM. The low-temperature remanence properties were measured on a Quantum Design Magnetic Properties Measurement System (MPMS).

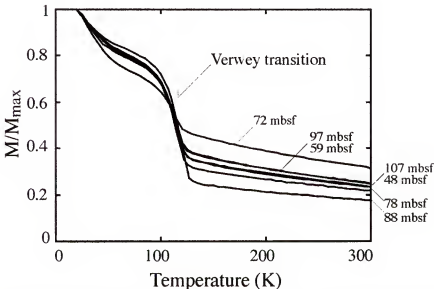


Figure 2-2. Thermal demagnetization at low temperature of the saturation isothermal remanent magnetization imparted at 20 K on 7 samples collected at Site 1101. The remanence loss at 110-120 K indicates the Verwey transition for magnetite.

The low-temperature measurements performed on 7 samples (randomly selected from 48 to 107 mbsf) show a significant drop in the intensity of magnetization around 110-120 K, corresponding to the Verwey transition of magnetite (Figure 2-2). No other low-temperature transition was observed. This indicates that magnetite is the main

mineral carrier of the magnetization in these sediments (Figure 2-2). The hysteresis loops obtained for 62 gelatin capsule samples have been compiled in Figure 2-3a. The shape of these hysteresis loops, as well as the values of the coercivity are compatible with those of magnetite. Calculation of the coercivity of remanence over coercivity (H_{cr}/H_c) and saturation remanence over saturation magnetization (M_{rs}/M_s) indicate a pseudo-single domain state for the magnetite grains (Day et al. 1977) (Figure 2-3b), except for one sample which is located in the multi-domain field on a “Day-plot” (Figure 2-3b).

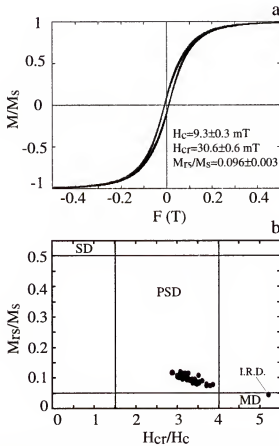


Figure 2-3. Rock magnetic study of 62 samples collected at Site 1101 (a) Hysteresis loops. The magnetic moments are normalized by their values at saturation. (b) Magnetic grain size distribution, as indicated by variations in the hysteresis parameters (Day et al. 1977). SD= single domain; MD= multidomain, and PSD= pseudo-single domain. IRD= Ice-rafted debris.

This sample (122.45 mbsf) was taken from an interval containing coarser-grained ice-rafted debris (IRD).

Magnetostratigraphy

The natural remanent magnetization (NRM) of the U-channel samples was measured at 2-cm intervals and was stepwise alternating field (AF) demagnetized at 20, 30, 40, 50, 60, and 80 mT peak values, using the 2-G Enterprises magnetometers located at the Institut de Physique du Globe de Paris and at the University of Florida.

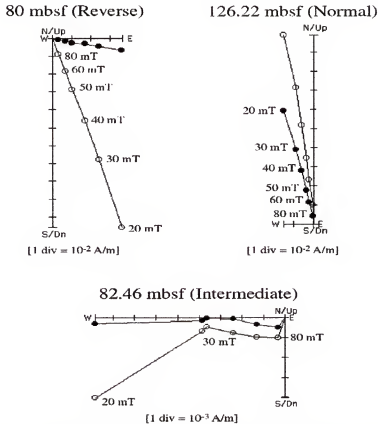


Figure 2-4. Typical examples of orthogonal projection (Zijderveld) plots for samples taken in reverse and normal polarity intervals, and during a polarity reversal. Open and closed symbols represent projections of vector end-points onto the vertical and horizontal planes, respectively. The plots show clear single-component directions of the NRM during periods of stable polarity, and no apparent drilling overprint after demagnetization at 20 mT.

We used the standard least-squares method to determine the principal components of paleomagnetic directions defined in the 20-80 mT interval (Kirschvink 1980). Unfortunately, the declination was not azimuthally oriented during drilling. The paleomagnetic inclination is, however, sufficient to establish a clear succession of polarity zones down to below the Olduvai subchron (Figure 2-5). The distribution of inclination values is bimodal, with two maxima located at -75° (normal polarity) and $+78^{\circ}$ (reverse polarity), which are close to the values of $\pm 76.5^{\circ}$ expected for a geocentric axial dipole field for a site at this latitude. Values of the maximum angular deviation (MAD) associated with our calculation of the principal components are for the most part lower than 5° , which demonstrates the overall quality of the directional data. The Brunhes/Matuyama polarity reversal occurs at 54.99 mbsf, the Jaramillo subchron is present over the interval 70.96-76.15 mbsf, and the Olduvai subchron is recorded between 121.25 mbsf and 126.97 mbsf. These depths are similar to those determined during shipboard investigations (Shipboard Scientific Party 1999).

We also observed two thin intervals with anomalous directions below the Jaramillo subchron (at 77.2-78.5 mbsf and 80.9-82.5 mbsf), hereafter referred to as Event 1 and Event 2 (Figure 2-5). Using a linear interpolation from the base of the Jaramillo subchron (1.07 Ma) to the top of the Olduvai subchron (1.77 Ma) (Cande and Kent 1995), we obtained ages of (1.09-1.11) Ma for Event 1 and (1.14-1.17) Ma for Event 2. Event 2 is likely to be the Cobb Mountain polarity interval, for which Shackleton et al. (1990) gave an age of 1.19 Ma by correlation of ODP Site 677 and DSDP Site 609. A similar succession of events has been observed in sediments from the California Margin (Guyodo et al. 1999), where the event between the Cobb Mountain and the Jaramillo subchrons has

been attributed to the Punaruu event, originally recorded in three lava flows from the Punaruu Valley in Tahiti (Singer et al. 1999). Our study suggests that two short geomagnetic events preceded the onset of the Jaramillo subchron at least locally over the Antarctic Peninsula, with a timing similar to the succession of events recorded in the Pacific (Guyodo et al. 1999).

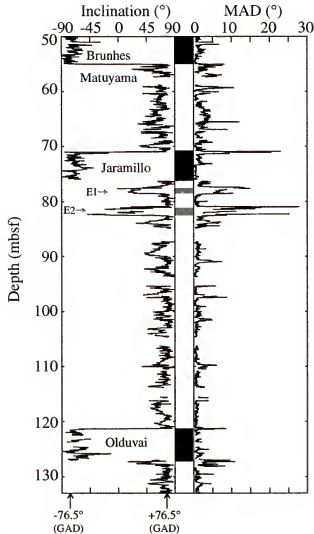


Figure 2-5. Inclination variations and maximum angular deviation (MAD) at Site 1101. Values of the MAD are generally lower than 5°, except during polarity transitions and short polarity intervals (E1= Event 1, E2= Event 2). The geocentric axial dipole (GAD) field inclinations for the site latitude ($\pm 76.5^\circ$) are also shown.

Time Scale

Oxygen isotope analysis was not possible at Site 1101 because of the overall low biogenic carbonate content, thus constraining us to date these sediments by other means. An initial time scale was derived from the magnetostratigraphy (Figure 2-5), using the ages of Cande and Kent (1995). This yielded mean sedimentation rates of 8.8 cm/kyr for the period 0.7-0.99 Ma, and of 6.1 cm/kyr for the period 0.99-2.1 Ma. A lower sedimentation rate of 3.1 cm/kyr was found for the Olduvai subchron, suggesting the possible presence of a hiatus or at least large variations in sedimentation rates in this interval. Considering the depositional setting in this region, the sedimentation rates are probably variable throughout the cored interval, possibly varying on a glacial/interglacial time scale.

Shipboard analyses showed that part of the magnetic susceptibility (κ) variations could be related to changes in the silica and carbonate content of the sediment, because susceptibility minima were generally associated with intervals of higher biogenic content (Shipboard Scientific Party 1999). This suggests that κ is primarily responding to variable dilution of terrigenous material with biogenic material. Consequently, because the biogenic content at Site 1101 varies with climatic periods (Shipboard Scientific Party 1999), first order variations of the U-channel magnetic susceptibility (κ) should correlate with climatic proxies. Therefore, we have refined our time scale by correlating the magnetic susceptibility to the benthic $\delta^{18}\text{O}$ target curve of ODP Site 677 (Shackleton et al. 1990). The correlation is shown in Figure 2-6, along with the location of CaCO_3 maxima, which indicate warmer periods (Shipboard Scientific Party 1999). The major

variations displayed by the susceptibility record can be matched fairly accurately to the $\delta^{18}\text{O}$ record, although uncertainties remain over shorter time-scales.

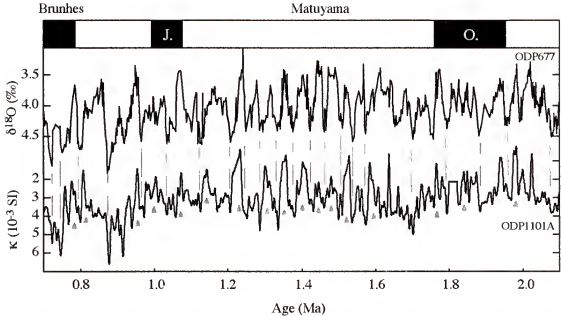


Figure 2-6. Correlation of the u-channel magnetic susceptibility record from Site 1101 to the benthic $\delta^{18}\text{O}$ record from ODP Site 677 (Shackleton et al. 1990). The correlation is suggested by gray lines. The gray triangles indicate the stratigraphic location of warmer climatic intervals inferred in part from peaks in the shipboard CaCO_3 record (Shipboard Scientific Party 1999).

Relative Paleointensity

The bulk magnetic parameters were measured at 2-cm stratigraphic intervals using 2G-Enterprises cryogenic magnetometers located in shielded rooms in the paleomagnetic laboratories at the University of Florida and at the Institut de Physique du Globe de Paris. An anhysteretic remanent magnetization (ARM) was imparted to the U-channel samples using a peak AF of 100 mT and a 0.05 mT DC bias field, and then was demagnetized at peak fields of 20, 30, 40, and 60 mT. The ratio of the susceptibility of ARM (κ_{arm} , ARM normalized by the bias field) over magnetic susceptibility (κ) was then computed. When dealing with magnetite, $\kappa_{\text{arm}}/\kappa$ varies inversely with magnetic grain

size, and so can be used to monitor down-core changes in magnetic grain size. In addition, a saturation isothermal remanent magnetization (SIRM) was imparted using a 1 T field.

The down-core variations of these parameters are shown in Figure 2-7. ARM, κ , and SIRM are believed to primarily reflect down-core changes in concentration of magnetic particles in the sediment (Tauxe 1993). It has been proposed that bulk magnetic parameters should vary by less than an order of magnitude in order to obtain useful paleointensity proxies (Tauxe 1993; King et al. 1983), which is not the case in the present study. For instance, ARM values vary by almost a factor of 20 throughout the entire record.

However, most of this variability is due to large amplitude changes below 78 mbsf, where there is a 50% down-core increase of the mean value of the NRM. The interval between 50 and 78 mbsf contains less variability in NRM intensity than the underlying sediment. This change is also seen to some extent in the κ_{arm}/κ ratio, which indicates a slightly finer average grain size for the interval 78-133 mbsf. These changes are probably sufficient to induce a shift in the response of remanence parameters to the applied field, and therefore these two depth intervals should be treated separately. In addition, the lower interval (78-133 mbsf) contains more regions of sediment disturbance (essentially at the top of cores), which make it difficult to obtain a complete geomagnetic record for this part of the record. For the study of relative paleointensity at Site 1101, we consequently restricted our investigation to the depth interval between 50 and 78 mbsf. Over this interval, the ARM varies by less than a factor of 6, which is appropriate for paleointensity determinations (Tauxe 1993).

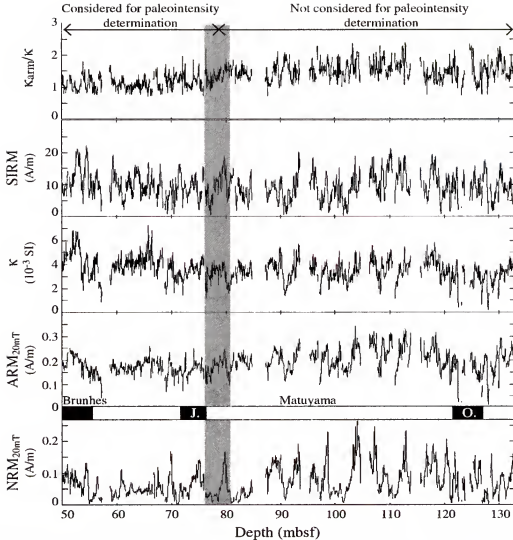


Figure 2-7. Bulk magnetic parameters for Site 1101. From bottom to top: down-core variations of the NRM demagnetized at 20 mT, ARM demagnetized at 20 mT, κ , SIRM, and κ_{arm}/κ . Overall, ARM varies by a factor greater than 20, which is more than usually considered acceptable for paleointensity determinations (Tauxe 1993). Over the interval 50-78 mbsf, however, ARM varies by less than a factor of 6, within the acceptable range.

In order to construct a relative paleointensity record, one must correct for variations in concentration of remanence (NRM) carrying grains. This is done by selecting the magnetic parameter (i.e., ARM, κ , or SIRM), that provides the best measure of the concentration of the magnetic grains that carry the NRM. We attempt to ascertain this using coherence functions between the magnetic parameters (ARM, κ , and SIRM)

and the paleointensity determined from normalizing the NRM by these parameters (Figure 2-8).

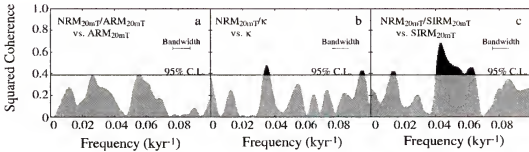


Figure 2-8. Coherence function between (a) ARM, (b) κ , and (c) SIRM, and the paleointensity proxies obtained by normalizing the NRM with these parameters for the interval 50-70 mbsf. Coherence above the 95% confidence values level are shown in black.

In principle, when the normalization is appropriate, the relative paleointensity is not correlated to the bulk rock-magnetic parameter used to normalize the NRM, and the values of the coherence should be lower than the 95% confidence level (Tauxe 1993). Squared coherence values lie above the confidence level over specific frequency intervals for the susceptibility normalization (Figure 2-8b). Much higher values of the squared coherence, and more spread over the frequency domain, are found for the SIRM normalization. Some problems were encountered when measuring the SIRM, due to the fact that the dynamic range of the magnetometer was sometimes exceeded when the intensity gradient was large. Therefore, some caution should be used when dealing with SIRM magnetization at this site. The lowest squared coherence occurs for the ARM normalization, indicating that it is the best choice, even though there are some frequency intervals over which the coherence is close to the significance level. The use of ARM as the normalizer can be further validated by comparing paleointensity estimates obtained with the ratios $\text{NRM}_{20}/\text{ARM}_{20}$, $\text{NRM}_{30}/\text{ARM}_{30}$, and $\text{NRM}_{40}/\text{ARM}_{40}$ (Figure 2-9). They

show nearly identical variations, which confirm the match between the coercivity spectra of the ARM and the NRM over the range of peak AFs. Therefore, we consider the ratio NRM/ARM to provide the best estimate of relative paleointensity at Site 1101. We used the average of the three ARM normalizations as our paleointensity proxy (Figure 2-9).

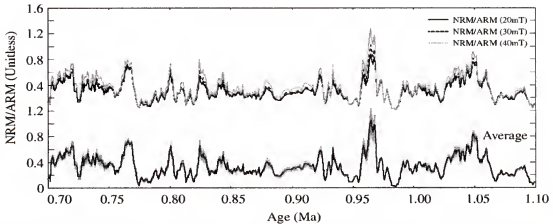


Figure 2-9. Paleointensity proxies obtained by dividing the NRM demagnetized at 20, 30, and 40 mT by ARM demagnetized at 20, 30, and 40 mT (top), and the arithmetic mean of the three normalizations (bottom). The standard deviation associated with the mean is plotted in gray.

Comparison with Other Paleointensity Records

One way of verifying the overall quality of a sedimentary paleointensity record is to compare it with other paleointensity curves available for the same time interval. In Figure 2-10, the paleointensity record obtained at ODP Site 1101 is compared with a record obtained at ODP Site 983 (ODP983) (Channell and Kleiven 2000) and a compilation from the Pacific Ocean (VM93) (Valet and Meynadier 1993). The long-term features present in the paleointensity record at Site 1101 are also observed in the two other paleointensity records. All records show a relatively sharp increase in the paleointensity after the geomagnetic reversals at the onset and termination of the

Jaramillo subchron, and at the onset of the Brunhes Chron. Overall, most of the variations with wavelengths of the order of a few tens of thousand years can be correlated between Sites 1101 and 983 (Figure 2-10). The correlation is poorer with VM93, and is also less easy to establish between ~0.82 Ma and ~0.9 Ma. The high-frequency variations are more difficult to correlate from one record to another, due to differences in the resolution and possible time scale discrepancies between records.

Most of the long-term variations seen in contemporaneous paleointensity records from the North Atlantic and Pacific Oceans are reproduced by our paleointensity record, and the main differences seem to appear as amplitude modulations of the paleointensity. Therefore, we attribute a common geomagnetic origin to the features observed in our paleointensity record. Some of the differences with other records could be due to failure in removing some of the non-geomagnetic signal present in the record, or uncertainties in chronologies (Guyodo and Valet 1996; Roberts et al. 1997; Brachfeld and Banerjee 2000). The best approach is probably to compare our record with a database integrating paleointensity records of resolution comparable with that at Site 1101, and corresponding to different regions of the globe and to different lithologies. This type of comparison is tenuous for the 0.7-1.1 Ma interval, because few records exist with reasonably good age control. However, some answers may be provided by a study of the short interval 0.95-1.1 Ma, which includes the Jaramillo subchron. This interval is characterized by sharp paleointensity features, and a time scale that is relatively well constrained by the presence of two geomagnetic reversals. Nine paleointensity records corresponding to different sedimentary environments are shown in Figure 2-11. There are six sites located in the Pacific Ocean (ODP1021, (Guyodo et al. 1999); VM93, (Valet and Meynadier 1993);

S98, (Sato et al. 1998); ODP1010C, (Leonhardt et al. 1999); KK78030, (Laj et al. 1996; Verosub et al. 1996); KT99 (Kok and Tauxe 1999)), one in the Indian Ocean (MD940, (Meynadier et al. 1994)), one in the Atlantic Ocean (ODP983, (Channell and Kleiven 2000)), and Site 1101.

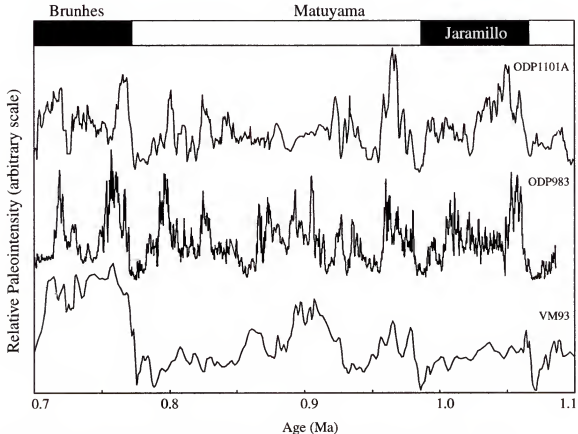


Figure 2-10. Comparison of the paleointensity profile obtained at Site 1101 with previously published records from the North Atlantic (Channell and Kleiven, 2000) and the Pacific (Valet and Meynadier, 1993) Oceans.

Most of these records show similar variations with minima that are synchronous within a few thousand years, although the amplitudes of specific peaks may vary from one record to another. Before performing a quantitative comparison, it is important to reduce the discrepancies related to resolution and dating. Over the time period considered, some of these curves have been dated solely by magnetostratigraphy

(ODP1010C, KK78030, ODP1021, S98, KT99), others by correlation of indirect climatic proxies to target curves (VM93, MD940, ODP1101), and only one using oxygen isotope techniques (ODP983). This leaves some margin for small readjustments of the age models for individual records.

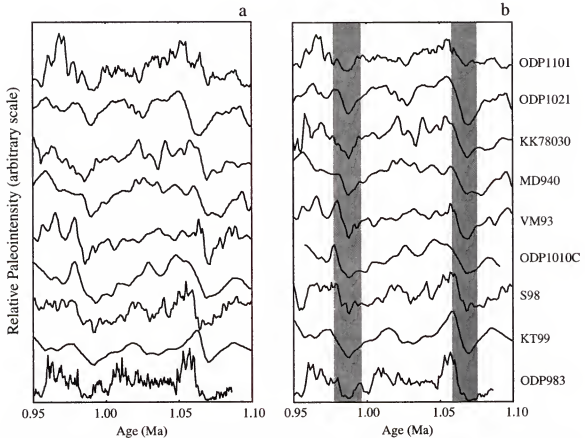


Figure 2-11. Comparison of records around Jaramillo. (a) Relative paleointensity at Site 1101 compared with eight other records over the time interval 0.95-1.1 Ma. All the records are placed on their published age models. (b) The same records after minor readjustment of the time scales around the reversals (in gray). The time scale of core ODP983 was taken as the reference. The records in (b) have been resampled at 1 kyr intervals.

The age model for ODP983 (Channell and Kleiven 2000) was derived from the tuning of precession cycles present in its $\delta^{18}\text{O}$ record to those of the ice volume model of Imbrie and Imbrie (1980), and this paleointensity record probably has the highest resolution chronology. For this reason, we correlated the major geomagnetic features of

all the paleointensity records to core ODP983. We tied the records using correlation points near the polarity reversals (Figure 2-11b), maintaining a consistent age for the two reversals at the boundaries of the Jaramillo subchron, where the intensity changes are the most dramatic. Other paleointensity features could have been matched, but the legitimacy of such a procedure would have been difficult to assess without the existence of independent control (i.e., oxygen isotope data). We also re-sampled the data every 1 kyr to obtain an even time sampling and to reduce the differences in resolution (although some differences remain), and normalized the data to equal mean and variance over the time interval common to all the records (0.958-1.086 Ma). The results of this operation are shown on Figure 2-11b, which is similar to Figure 2-11a.

A suitable procedure for evaluating the degree of reliability of specific records involves comparing each paleointensity record to the rest of the database. One statistical approach would be to perform a test similar to a jackknife. In order to do so, and to evaluate the amount of noise introduced by each of the nine paleointensity records in our database, we built nine distinct subsets of data, each time removing a different record from the database. For each subset of eight records, we calculated the relative difference between the average curve calculated with this particular subset and a reference curve constructed with all the records (Figure 2-12a, hereafter referred to as the Jaramillo Stack). This difference provides a measure of the bias introduced by the record that was removed from the database. If a significant change is noticed in the average curve when a specific record is removed from the database, it means that this record has a negative impact on the stack, and therefore does not fit well to the other records.

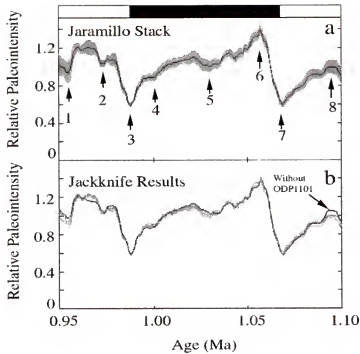


Figure 2-12. Results of the jackknife test performed on the paleointensity records shown in Figure 2-11. (a) Reference curve for the test. This curve corresponds to the arithmetic mean of the nine records in Figure 2-11b. The error bars (in gray) correspond to the standard error. The characteristic features of this stack are labeled with numbers. (b) Jackknife results showing the nine stacks obtained from nine subsets of paleointensity records. Each subset is obtained by removing a different record from the entire database. The result corresponding to the subset without core ODP1101 is shown in black. No outlier can be identified.

The nine paleointensity curves obtained by following this procedure are plotted in Figure 2-12b. From this figure, it is not possible to distinguish any outlier. The minimum difference between the average curves obtained with the nine subsets and the Jaramillo Stack was found with core KK78030 ($1.0 \pm 0.2\%$). The maximum difference was obtained with core KT99 ($1.5 \pm 0.2\%$) (Table 2-1). In addition, we calculated the correlation coefficients between the individual paleointensity records and the Jaramillo Stack. All the correlation coefficients are greater than 0.8 (Table 2-1), which indicates a strong correlation between the records, and attests to their geomagnetic origin.

Table2-1. Average differences (delta) between the Jaramillo Stack and the stacks calculated from nine subsets of paleointensity records.

Paleointensity records	Delta (%)	R
ODP1101	1.3 ± 0.2	0.8
ODP1021	1.2 ± 0.2	0.9
VM93	1.3 ± 0.2	0.8
ODP983	1.1 ± 0.1	0.9
MD940	1.2 ± 0.2	0.8
S98	1.1 ± 0.1	0.9
ODP1010C	1.3 ± 0.1	0.8
KK78030	1.0 ± 0.2	0.9
KT99	1.5 ± 0.2	0.8

Note: The uncertainties correspond to the standard error at the 95% level. The R values correspond to the correlation coefficients between individual paleointensity records and the Jaramillo Stack.

Conclusions

We have investigated the magnetic properties of a sedimentary sequence at ODP Site 1101 covering the time interval 0.7-2.1 Ma. The NRM of the sediment is carried by pseudo-single domain magnetite, and yielded a directional record allowing us to establish a magnetostratigraphy down to the Olduvai subchron. In the sediment underlying the Jaramillo subchron, two short geomagnetic events were observed at 1.09-1.11 Ma (Event 1) and 1.14-1.17 Ma (Event 2). Event 2 is identified as the Cobb Mountain polarity interval. Event 1, which occurred closer to the onset of the Jaramillo subchron, may be the same event as that observed on the California Margin (Pacific Ocean, Site 1021) and in the Punaruu Valley, Tahiti.

We obtained a record of relative paleointensity by normalizing the NRM with the ARM after demagnetization at 20, 30, and 40 mT, over the time interval 0.7-1.1 Ma. Comparison of the paleointensity record obtained at ODP Site 1101 with records from the North Atlantic and Pacific Oceans indicated that the variations recorded at Site 1101 are geomagnetic in origin. The quality of the record was additionally assessed by a jackknife

test over the time interval 0.95-1.1 Ma. This enabled construction of a composite record of relative paleointensity for the Jaramillo subchron, by compiling the geomagnetic features common to nine sites from different oceans (Figure 2-12a). Overall, the Jaramillo Stack displays the same variations as those documented in previous studies (Channell and Kleiven 2000; Leonhardt et al. 1999; Laj et al. 1996) (Figure 2-12a). The paleointensity variations can be correlated from one hemisphere to the other for this time interval, although features may vary in amplitude from one record to another. They reflect global variations of the geomagnetic dipole over the time span investigated here. Better definition of these features could be achieved by slightly shifting the individual records within the Jaramillo subchron, but the validity of such a procedure cannot be established with the existing age control. Paleointensity minima numbered 3 and 7 in Figure 2-12a are the most prominent features of this compilation, and correspond to the polarity reversals bounding the Jaramillo subchron. Recovery of field intensity post-reversal is abrupt and appears to occur within ~15 kyr. Additional records, with better age control and higher resolution will be needed in order to reduce the error bars, and extend the time domain explored by this type of compilation. With this in mind, the recovery of complete and well-dated sedimentary sequences from high latitudes will be crucial for developing the database necessary to test the various geodynamo models.

CHAPTER 3
WAVELET ANALYSIS OF RELATIVE GEOMAGNETIC PALEOINTENSITY AT
ODP SITE 983

Introduction

In the past ten years, more than 30 sedimentary records of relative paleointensity of variable resolutions and duration have been published (Channell et al. 1997, 1998, Channell and Kleiven 2000; Guyodo et al. 1999; Meynadier et al. 1992, 1994; Stoner et al. 1995, 2000; Tauxe and Shackleton 1995; Tric et al. 1992; Valet and Meynadier 1993; Yamazaki and Ioka 1995). This fast-growing database is believed to reflect the time evolution of the geomagnetic dipole field intensity, hence constraining the models aimed at describing the processes governing the geodynamo. Evidence for the reliability of sedimentary records of relative paleointensity is provided by the high degree of correlation between individual records from different regions of the world (Laj et al. 2000; Guyodo and Valet 1996, 1999; Channell et al. 2000). Additional proof comes from the covariance of these records with paleointensity proxies derived from cosmogenic radionuclides such as ^{10}Be and ^{36}Cl (Baumgartner et al. 1998; Frank et al. 20; Frank 2000). Since geomagnetic intensity may vary on a global scale, the use of relative paleointensity records as a correlative tool is of great interest. Relative paleointensity stratigraphy may offer a time resolution greater than $\delta^{18}\text{O}$ techniques, which could be of crucial importance for correlation and dating of climate proxy records in sediments. Integration of these paleointensity records (Laj et al. 2000; Guyodo and Valet 1999)

into composite records has provided target curves (NAPIS-75, Sint-200, Sint-800) for the last 800 thousand years. Significant refinement of these curves will be achieved with additional high quality records, and the routine use of quantitative methods of investigation such as jackknife techniques, coherence function spectrum, and in some cases wavelet analysis.

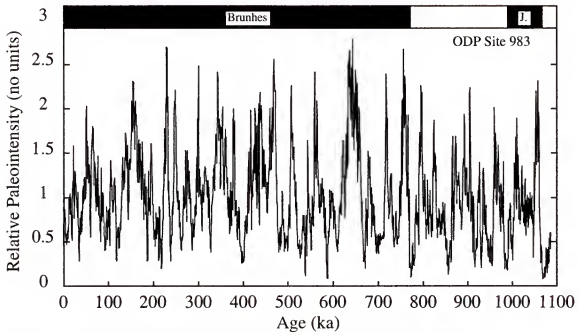


Figure 3-1. Relative geomagnetic paleointensity record at ODP Site 983.

The scope of this chapter is to present the wavelet analysis of a recently published record of relative paleointensity from Ocean Drilling Program (ODP) Leg 162 Site 983 (Channell et al. 1997, 1998, Channell and Kleiven 2000). Site 983 (60.4° N, 23.64° W) is of particular interest because it provided a high latitude, high resolution paleomagnetic record (average sedimentation rate of 12.3 cm/kyr), characterized by a high density of age calibration points. The magnetic properties were measured on U-channel samples (Tauxe et al. 1983), using the 2-G enterprises pass-through magnetometers located at Gif-sur-Yvette (France) and at the University of Florida (Weeks et al. 1993; Nagy and Valet

1993). The natural remanent magnetization (NRM), the anhysteretic remanent magnetization (ARM), and the isothermal remanent magnetization (IRM) were progressively alternating field demagnetized, and measured at each demagnetization step (Channell et al. 1997, 1998; Channell and Kleiven 2000). The magnetic susceptibility (k), the ARM, and the IRM were used to normalize the NRM for variations in concentration of magnetic grains and construct paleointensity proxies. Comparison of the three estimates for several demagnetization steps pointed to the ratio NRM/IRM as the best paleointensity proxy at this site (Channell et al. 1997, 1998; Channell and Kleiven 2000).

An initial spectral investigation of the ODP Site 983 paleointensity record was performed for the interval 0-725 ka (Channell et al. 1998). The power spectrum revealed the existence of significant power at the earth orbital eccentricity (0.01 kyr^{-1} , 100 kyr) and obliquity (0.0244 kyr^{-1} , 41 kyr) frequencies. A similar analysis was performed on the bulk magnetic parameters, and showed that the cycles at 100 kyr were present in all the records. The paleointensity signal at 100 kyr was therefore attributed to a lithologic overprint. In contrast, the 41 kyr cycles were not observed in the bulk magnetic parameters, and it was concluded that the obliquity cycles observed in the paleointensity record may be geomagnetic in origin, and that the geodynamo may be influenced by the orbital obliquity. Another spectral analysis on the interval 700-1100 ka yielded similar results (Channell and Kleiven 2000). The signal to noise ratio in the bulk magnetic parameters is however relatively low for these frequencies so that small intervals with significant power at orbital frequencies may have been missed by the initial Fourier analysis. Given the high resolution and superior age control in this record, it provides a unique opportunity to try spectral methods of greater resolution. The present study

concerns the entire paleomagnetic record, covering the last 1100 kyr (Figure 3-1). Over this interval, we applied wavelet analysis techniques in search of potential non-stationarities, and to investigate the possibility of previously undetected coherency between the paleointensity signal and the bulk magnetic parameters. The results presented in this chapter were published in the journal *Earth and Planetary Science Letters* (Guyodo et al. 2000).

Spectral Analysis

Global Power Spectrum

Figure 3-2 represents the global power spectrum calculated for the paleointensity and the IRM (normalizer) records, along with the associated coherence function (squared coherence and phase). The spectrum was obtained using the Blackman-Tukey method and a Bartlett window (Paillard et al. 1996). The power spectrum calculated for the 0-1100 ka paleointensity record reveals two maxima associated with frequencies close to those of the earth orbital parameters (Figure 3-2). A first significant peak is found at 0.01 kyr^{-1} (100 kyr), and a second broader peak is found between 0.021 kyr^{-1} (48 kyr) and 0.029 kyr^{-1} (35 kyr). In contrast to the first analysis performed over the interval 0-725 ka (2), the peak at 0.0244 kyr^{-1} (41 kyr) is a double peak (first maximum at 0.0240 kyr^{-1} and second at 0.0273 kyr^{-1}). This could be the result of some inaccuracies in dating, or the expression of the various dynamics of the system (e.g., different levels of climate overprint added to a stochastic geomagnetic signal, or real evolution of the time scales inherent to the geodynamo). As a check, we applied the same spectral analysis to the benthic and planktic $\delta^{18}\text{O}$ records which were used to construct the age model (Figure 3-3).

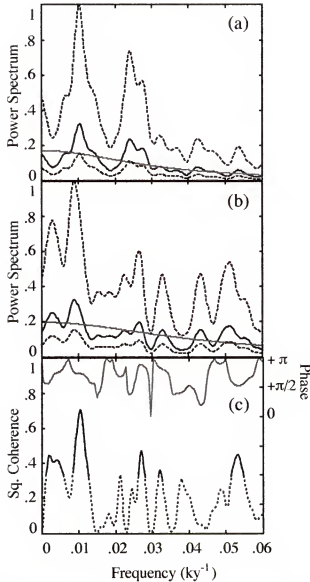


Figure 3-2. Power spectra of (a) the relative paleointensity record and (b) the IRM record at ODP Site 983. The sloping lines represent the best fit estimates for the background (red noise) spectra. The dashed lines correspond to the confidence limits at the 95% confidence level. (c) Coherence function (square coherence and phase) between the paleointensity record and the IRM. The dashed line corresponds to signals below the 95% confidence level

Those calculations yielded very clear power spectra, with a sharp peak at 41 kyr showing that the double peak observed in the paleointensity power spectrum is not due to dating inaccuracies. In addition, some coherency can be observed between the IRM and the paleointensity for periods close to the eccentricity and the obliquity.

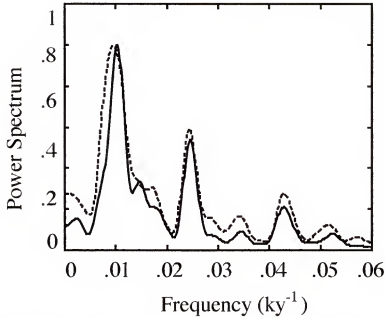


Figure 3-3. Power spectra of the benthic (solid line) and planktic (dashed line) $\delta^{18}\text{O}$ records at Site 983.

As already mentioned, no such coherency was observed in the previous spectral analyses of the data (Channell et al. 1998; Channell and Kleiven 2000), which might be due to the fact that we performed our analysis over a much longer interval. therefore slightly increasing the signal to noise ratio. However, the IRM spectrum is still very close to the one of red noise (Figure 3-2), suggesting some caution in the interpretation of this apparent coherence. A better understanding of the origin of these signals may arise from the reconstruction of the time evolution of the power spectrum.

Evolutionary Power Spectrum

One way of assessing the time evolution of a time series power spectrum is to compute the evolutionary power spectrum of that series, which can be represented as a color diagram displaying ages on the horizontal axis, frequencies on the vertical axis, and indexed colors for the power spectrum. We constructed the evolutionary spectrum of the ODP Site 983 paleointensity record by calculating the power spectrum of the time series

within a sliding window of 300 kyr width and a translation step of 50 kyr, using the same spectral method as for the global spectrum (Figure 3-4). The results show that the spectral content of the paleointensity record is time dependent.

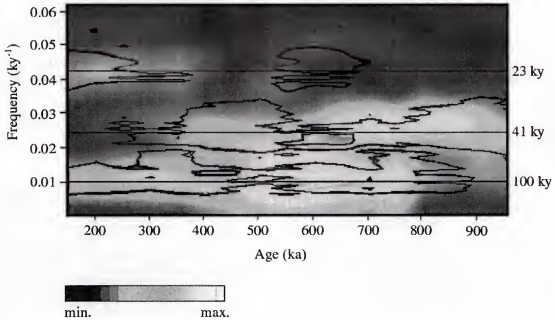


Figure 3-4. Evolutionary power spectrum of the paleointensity record at Site 983. The spectrum was obtained using a sliding window of 300 kyr width and steps of 50 kyr. The contour lines correspond to the best fit estimate of the background spectrum.

The last ~800 kyr is the only time interval when the signal corresponding to the eccentricity (100 kyr, 0.01 kyr^{-1}) is present. The bandwidth associated with the obliquity (41 kyr, 0.0244 kyr^{-1}) is observed only between ~400 ka and ~900 ka, and displays a frequency shift around ~600 ka. This observation accounts for the two peaks observed in the global power spectrum, which may be interpreted as a result of the time dependency of the power spectrum. However, it does not tell us about the origin of the signal, nor if these two peaks are the expression of the obliquity only, or a combination of several signals including the obliquity. The signal in this spectral band drops below the background spectrum (as defined by the red noise spectrum associated with this record)

around ~600 ka, over an interval of ~100 kyr. This indicates that the spectral content of the paleointensity record varies over time scales shorter than the window used to calculate the power spectra (i.e., 300 kyr). As a consequence, although the evolutionary spectrum represents an improvement relative to the global approach, it is inappropriate for resolving the small time scales present in this record.

A better resolution of the periodicity around 41 kyr could be obtained by reducing the size of the sliding window. However, it would generate aliasing of the lower frequencies and reduce the quality of the output at that scale. In order to solve this problem, we must use a method providing spectral information that is scale independent. The wavelet transform is a good candidate for such a task (Daubechies 1992; Torrence and Compo 1998; Lau and Weng 1995).

Wavelet Analysis

Description of the Method

Wavelet analysis provides an automatic localization of specific behaviors such as cyclic patterns or discontinuities, both in time and frequency (Daubechies 1992; Torrence and Compo 1998). In contrast to the Fourier transform, which is computed using a single time window of constant width, the wavelet transform is a multi-scale method that uses narrow windows at high frequencies and wide windows at low frequencies (Lau and Weng 1995).

Wavelet analysis contrasts strongly with the classical Fourier transform and windowed spectral analysis, which do not detect temporal discontinuities, are not able to distinguish between continuous low-amplitude and non-stationary high-amplitude

signals, and do not provide information on the temporal persistence of periodicities. The continuous wavelet transform of a time series $f(t)$ is defined as:

$$W_{\Psi}(a, b) = \frac{1}{\sqrt{a}} \int_{\tau} f(t) \cdot \Psi\left(\frac{t-b}{a}\right) dt \quad (\text{Eq. 3-1})$$

where Ψ is a base wavelet characterized by a length much shorter than the time series $f(t)$, and a , b , and T correspond to the dilatation scales, translation steps, and time length of the wavelet transform, respectively. The wavelet $\Psi(t)$ must be a function with compact support and zero mean. The second property (admissibility condition) ensures that $\Psi(t)$ has a wiggle (i.e., is wave like), and the first ensures that it is not a sustaining wave. Here, we use the Morlet wavelet (Daubechies 1992; Morlet et al. 1982) because its shape is similar to a periodic sinusoidal function, suitable for investigating periodicities (Figure 3-5). The Morlet wavelet $\Psi(t) = \pi^{-1/4} e^{i\omega_0 t} e^{-t^2/2}$ (in our case $\omega_0 = 5$) is a complex valued function enabling extraction of information on both the amplitude and phase of the process being analyzed. The normalizing constant $1/\sqrt{a}$ is chosen so that $\Psi_a(t)$ has the same energy for all scales. The scale parameter (or dilatation factor), a , determines the characteristic frequencies at which the wavelet transform is computed. In our case, the dilatation scales were chosen so that the equivalent Fourier periods are given by $2^{k\delta k} t_0$, where t_0 is the sampling rate of the time series (Fourier period = 1.224 a) (Torrence and Compo 1998). The parameter $k\delta k$ is chosen so that it is possible to cover the Fourier domain of interest (here the one containing periods of 23 kyr, 41 kyr, and 100 kyr) with an appropriate resolution (Torrence and Compo 1998). A reading of the wavelet power spectrum can be obtained by constructing a color diagram with the ages on the horizontal axis and the scales (or the equivalent Fourier periods) on the vertical axis; the modulus of the wavelet transform being represented by colored patches (Torrence and Compo 1998).

This type of diagram is therefore comparable to an evolutionary power spectrum, and can be revealing about the structure of a particular process. The main difference between the wavelet and the Fourier decompositions is in the support of the respective basis functions. The wavelet transform coefficients are influenced by local events, while the Fourier coefficients are influenced by the function in its entire domain. This makes the wavelet spectrum a better measure of the variance attributed to localized events (Lau and Weng 1995).

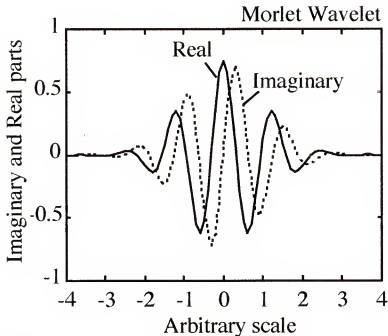


Figure 3-5. The Morlet wavelet used to compute the wavelet transform. The solid line corresponds to the real part of the wavelet function, and the dashed line to its imaginary part.

Figure 3-6 represents the wavelet power spectra of two synthetic time series $x_1(t)$ and $x_2(t)$. The first series $x_1(t)$ is a modulated function containing periodic signals at 41 kyr and 100 kyr. The second function $x_2(t)$ was constructed from a sinusoidal function of period 41 kyr in quadrature with $x_1(t)$. The wavelet power spectra in Figure 3-6 show the modulations characterizing $x_1(t)$, as well as the time intervals over which the 41 kyr and

the 100 kyr signals are actually present. In order to facilitate the interpretation of this type of diagram, one can define a level above which a maxima in the wavelet spectrum or in the cross-wavelet power is statistically significant. It has been shown that each point in the wavelet power spectrum is statistically distributed as a χ^2 distribution with two degrees of freedom about the background spectrum (Torrence and Compo 1998). The confidence level at each scale is therefore the product of the background spectrum and the desired significance level (for instance 95% confidence) from the χ^2 distribution. Here, the background spectrum is determined by calculating the time-average of the wavelet spectrum (Torrence and Compo 1998).

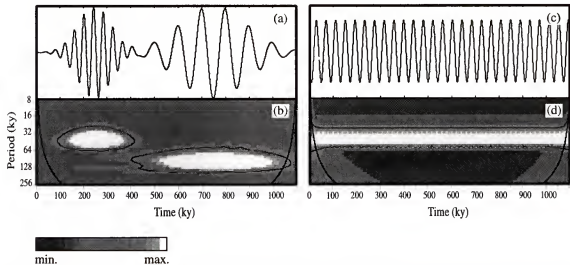


Figure 3-6. Examples of wavelet spectra obtained for synthetic time series, with the ages on the horizontal axis and the equivalent Fourier periods on the vertical axis; the modulus of the wavelet transform being represented by indexed colors. This type of diagram is therefore comparable in its representation to an evolutionary power spectrum. The first series contains (a) two periodic signals (41 kyr, 100 kyr) over different intervals, which are identifiable as white patches on the wavelet spectrum (b). The second series (c) has a single frequency, which yielded a clear wavelet spectrum (d). The contour lines represent the confidence level at 95%. The thick black lines on the left and right edges of the spectra indicate the regions of the diagram where the edge effects become important.

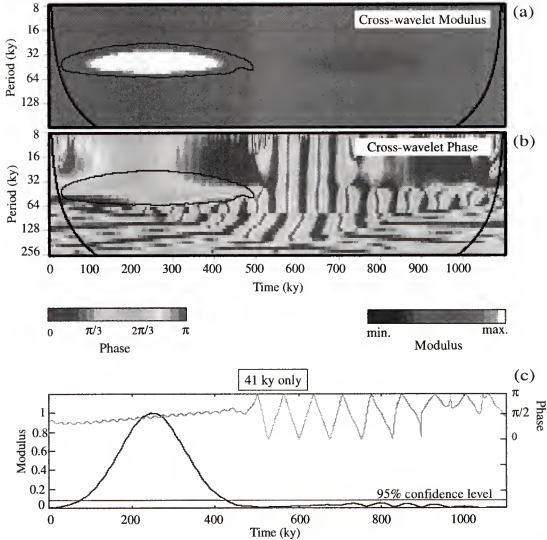


Figure 3-7. Cross-wavelets for the same two time series as in Figure 3-6. (a) Spectrum. (b) Phase. The two series are coherent only over the first half of the record, over which they display a phase lag of $\pi/2$. (c) Cross-wavelet spectrum and phase for the 41 kyr Fourier period only.

Similarly, the confidence levels of the cross-wavelet spectrum can be derived from the square root of the product of two χ^2 distributions (Torrence and Compo 1998; Jenkins and Watt 1968). In addition to the wavelet power spectrum, it is possible to construct the cross-wavelet spectrum $W^{xy}_\psi = W^x_\psi W^{y*}_\psi$ of two time series $x(t)$ and $y(t)$ from their respective wavelet transforms W^x_ψ and W^y_ψ (W^{y*}_ψ is the complex conjugate of W^y_ψ). Subsequently, cross-wavelet power (modulus) and phase can be extracted. Local

maxima in power provide information about the scales at which coherent events have a significant contribution. In Figure 3-7 we present the cross-wavelet power and phase of the synthetic series $x_1(t)$ and $x_2(t)$ from Figure 3-6. The diagrams show that the covariance between the two series is limited to the first half of the records (i.e. where the 41 kyr period exists in both series). In addition, the cross-wavelet phase gives the phase relationship between the two series (here equal to $\pi/2$), which is stable only over the interval containing the 41 kyr signal. If one wants to focus on a specific scale (or the equivalent Fourier period), the cross-wavelet spectrum and phase can be represented for this particular scale only (Figure 3-7c). This corresponds to a reading of the information provided by Figures 3-7a and 3-7b along a horizontal line placed at 41 kyr.

Wavelet Power Spectrum of ODP Site 983 Paleointensity Record

A wavelet transform of the relative paleointensity record at ODP Site 983 was computed. The wavelet power spectrum, modulus of the wavelet transform, is shown on Figure 3-8a. Essentially, the features initially observed in the evolutionary power spectrum are depicted with more detail. The signal for the 100 kyr period (possibly the eccentricity signal) is restricted to the last ~750 kyr and shows some modulations, with three maxima centered at ~150 ka, ~400 ka, and ~650 ka. The signal at 41 kyr (obliquity) is observed over relatively short periods of time. Three main intervals can be distinguished: 400-550 ka, 650-825 ka, and 950-1100 ka. Furthermore, the apparent shift in frequencies observed in the evolutionary power spectrum does not appear on the wavelet spectrum. In contrast, it reveals the existence of a complex structure over the interval 400-550 ka, characterized by scales with equivalent Fourier periods ranging from 10 to 70 kyr. Therefore, only a small fraction of the intensity seems to be carried by the 41 kyr period signal over this interval, which accounts also for the shift observed in the

evolutionary power spectrum. A few patches corresponding to the 23 kyr signal (precession) are also present in the wavelet power spectrum, essentially around ~250 ka, ~500 ka, and ~1050 ka. These intervals were barely detected by the evolutionary spectrum. In addition, several small-scale features of short duration are scattered though the wavelet spectrum. These features correspond to intervals in the paleointensity record characterized by large amplitude variations such as for instance the intervals 30-60 ka, or 100-160 ka (Figures 3-1 and 3-8). These intervals of major change in relative paleointensity do not correspond to parts of the paleointensity records containing frequencies similar to the orbital obliquity. In order to understand the origin (climatic overprint or orbital forcing in the geodynamo) of the periodic signals detected by the wavelet transform, we performed the same analysis on the IRM (Figure 3-8b), which was used to normalize the NRM to yield the paleointensity proxy. As for the spectral method involving the calculation of coherence functions, a match between the wavelet spectrum of the paleointensity record and the one of the IRM indicate an incomplete normalization of the NRM. We also calculated the wavelet transform of the ratio ARM/k (Figure 3-8c), which can be used as a proxy for relative changes in grain size of magnetite, the principal remanence carrier. Figures 3-8b and 3-8c show significant power in frequencies corresponding to the orbital parameters over time intervals similar to those of the paleointensity record (Figure 3-8a). The existence of some intervals over which the IRM and the paleointensity records depict similar wavelet power spectra suggests that part of the lithologic component of the NRM was not completely removed by the normalization with IRM. The similarity between the paleointensity record and ARM/k (Figure 3-8c) suggests that the NRM does not depend on the magnetic field and the magnetic

concentration alone, but also on the magnetic grain size. This would explain why the IRM, influenced by the concentration of a particular grain size fraction, and not as sensitive to grain size as ARM/k, would not be able to fully normalize the NRM at orbital frequencies.

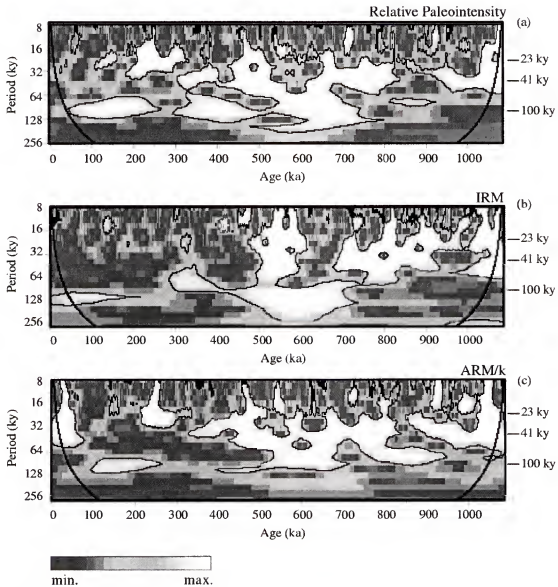


Figure 3-8. Wavelet spectra. (a) Wavelet spectrum of the paleointensity record at Site 983, showing the time intervals where significant power exists at frequencies corresponding to the earth orbital parameters. (b) Wavelet spectrum of IRM. (c) Wavelet spectrum of the ratio ARM/k.

A quantitative assessment of this covariance can be obtained by calculating the cross-wavelet spectrum between the paleointensity record and the magnetic parameters, following the same philosophy as when computing coherence function spectra from the global spectral analysis.

Cross-Wavelet Spectra

Cross-wavelet spectra were calculated between the relative paleointensity record and the IRM and the ratio ARM/k. Cross-wavelet powers and phases were subsequently extracted. Instead of plotting these results in the form of contoured diagrams we have selected only the relevant scales for clarity (i.e., 23 kyr, 41 kyr, and 100 kyr). The results show significant covariance between the relative paleointensity record and both the IRM and the ratio ARM/k in specific intervals of the time series (Figure 3-9). For each frequency, this covariance is observed over the same time intervals as those showing significant power in the paleointensity. When a high correlation is observed, the paleointensity signal tends to have inverse phase with respect to IRM, while it is in phase with ARM/k. This may be the consequence of a secondary dependency of the NRM on the magnetic grain size. In order to test the plausibility of this hypothesis, we constructed a simple synthetic model in which the NRM was simulated by a time series $S1(t) = (0.8 S2(t) + 0.2 S3(t)) S4(t)$, where $S2(t)$ represents a model of magnetic concentration (depicted by the IRM) and $S3(t)$ a model of magnetic grain size (depicted by the ratio ARM/k), and $S4(t)$ the geomagnetic field. The two other series, $S2(t)$ and $S3(t)$ were constructed from red noise spectra with the addition of two sinusoidal signals of periods 100 kyr and 41 kyr. The synthetic paleointensity record was then calculated by normalizing $S1(t)$ with $S2(t)$ (Figure 3-10).

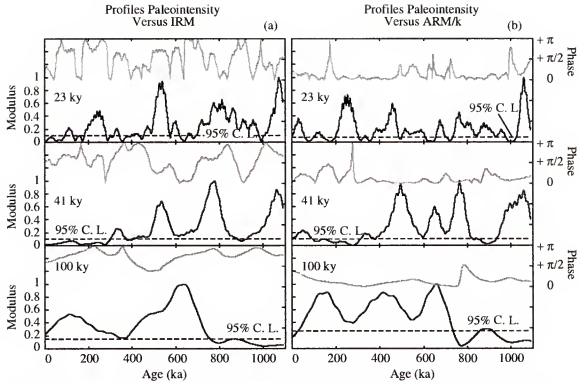


Figure 3-9. Cross-wavelet spectra (back lines=power and gray lines=phase) of (a) the paleointensity record versus the IRM and (b) the paleointensity record versus the ratio ARM/k. We selected the scales corresponding to the earth's orbital parameters.

We also calculated the coherence functions between the paleointensity model $S5(t)$ and the parameters $S2(t)$ and $S3(t)$. Figure 3-10 indicates that a slight grain size dependency of the NRM would induce significant covariance of the relative paleointensity with IRM, as well as with the ratio ARM/k. In addition, the paleointensity would be in phase with the ratio ARM/k and in opposition of phase with the IRM. The coherence functions were calculated over the entire interval, since the periodic signals built into the series were steady, and provided results showing strong correlations. There is no doubt that increasing the complexity of the model, by involving modulation of the periodic signals, different noise spectra, and abrupt changes in lithology and sedimentation rates would provide more realistic results such as those presented in Figure

3-9. In any case, this very simple model provides a good, and rather simple explanation of the cross-wavelet spectra obtained for the Site 983 relative paleointensity record.

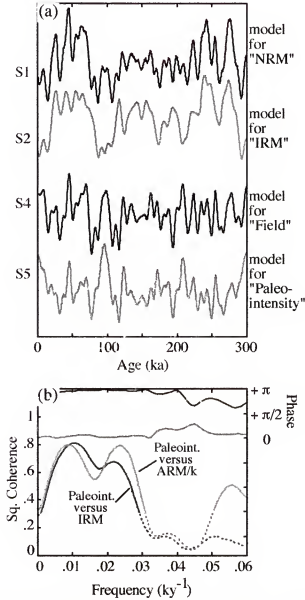


Figure 3-10. Synthetic model aimed at explaining the observed coherence between the paleointensity record and the magnetic properties. (a) Models for $S1(t)$ (NRM), $S2(t)$ (IRM), $S4(t)$ (geomagnetic field), and $S5(t)=S1(t)/S2(t)$ (relative paleointensity). Notice that the paleointensity variations are very similar to the model for geomagnetic variations. (b) Coherence transforms of model paleointensity versus model IRM (in black) and versus model ARM/k.

One positive outcome of this model is that an incomplete normalization of the NRM over specific time intervals would not diminish the overall character of the paleointensity record. Indeed, the series S4(t) (field model) and S5(t) (paleointensity model) display very similar features, and are correlated with a high correlation coefficient of 0.75 (Figure 3-10). This conclusion comes in support of other studies (Valet and Meynadier 1993; Guyodo and Valet 1996, 1999; Stoner et al. 1998) showing that paleointensity records with different lithologies and sedimentation histories, including the present dataset, can be correlated over high distances with a large degree of confidence.

Conclusion

The existence of periodic signals embedded into the paleointensity record at ODP Site 983, which was reported by previous studies, is confirmed (Channell et al. 1997, 1998; Channell and Kleiven 2000). These signals correspond to the earth orbital eccentricity (100 kyr), obliquity (41 kyr), and precession (23 kyr). Calculation of the evolutionary power spectrum for the paleointensity record over the interval 0-1.1 Ma established the non-stationarity of these periodic signals, which display amplitude variations and are restricted to specific time intervals. The duration of these amplitude modulations appear to be smaller than the sliding window used to construct the evolutionary spectrum (300 kyr), calling for the use of more suitable spectral methods.

The use of wavelet analysis allowed us to define with greater precision the intervals over which the orbital frequencies are present in the record. The signal for the 100 kyr period (eccentricity) is restricted to the interval 0-750 ka and shows some modulations, with three maxima centered at ~150 ka, ~400 ka, and ~650 ka. The signal at 41 kyr (obliquity) is observed over relatively short periods of time. Three main intervals

can be distinguished: 400-550 ka, 650-825 ka, and 950-1100 ka. The apparent absence of the 100 kyr period prior to ~750 ka, in the so-called 41-kyr world, may reflect the diminished influence of the eccentricity in climate proxy records. Other significant scales of variability were also recognized in the paleointensity record, resulting from the high complexity of the field which seems to be essentially non-stationary (Sato et al. 1998). For the orbital frequencies, the paleointensity record shows significant and stable covariance with the IRM and ARM/k over specific intervals of the record. This did not appear in previous spectral investigations of the paleointensity record (Channell et al. 1998; Channell and Kleiven 2000) performed using standard spectral methods. Our study suggests that it is probably due to the limitations imposed by the global Fourier analysis, which is not always able to detect low-amplitude, locally-distributed signals. Our wavelet analysis suggests the presence of a secondary lithologic overprint in the paleointensity record due to an incomplete normalization of the NRM. The results seem to be explained by simple models involving a slight magnetic grain size dependency of the NRM. The model shows also that the lithologic overprint does not drastically modify the paleointensity record, which remains very similar to the actual field model (Figure 3-10).

Quantification of the amount of climatic overprint in the paleointensity record is not an easy task, nor is the normalization of this secondary component. In an attempt to estimate this overprint, we removed the orbital signals from the paleointensity record. As a first step, we extracted the wavelet components at (23 ± 5) kyr, (41 ± 5) kyr, and (100 ± 5) kyr. Then, we weighted the wavelet components with the cross-wavelet profiles of paleointensity versus ARM/k obtained for those frequencies, in order to restrict the filtering to the time intervals where a covariance between the two records exists.

Evidently, the signal extracted contains information on both the overprint and the geomagnetic field. Indeed, the true geomagnetic signal contains variability at these time scales, as would any stochastic signal, which means that its power spectrum overlaps the one of ARM/k. The output signals were then subtracted from the initial paleointensity variations. Figure 3-11a shows the power spectrum of the resulting filtered signal, which does not seem to have any dominant Fourier period, compared with the global power spectrum of the original paleointensity record. The filtered paleointensity record does not seem to differ considerably from the initial record (Figure 3-11b), with an overall difference of about ~7%.

The main changes reside in a reduction of some of the large amplitude variations present in the initial paleointensity record (Figure 3-11b). The wavelet transform of the filtered paleointensity record (Figure 3-11c) shows patches that are more uniformly distributed than for the initial paleointensity record (Figure 3-8a). In particular, the regions of the spectrum corresponding to higher frequencies appear more clearly. This indicates the lesser dominance of specific oscillations, and that the filtered signal can be compared to a stochastic process.

However, the extracted wavelet components are likely to contain some true geomagnetic signal over some intervals, or may have ignored some of the lithologic overprint (due to the restricted bandwidth of the filtering). An actual correction of the paleointensity signal would require quantification of the dual dependency of the NRM on the IRM and ARM/k, which is probably not constant throughout the time interval investigated.

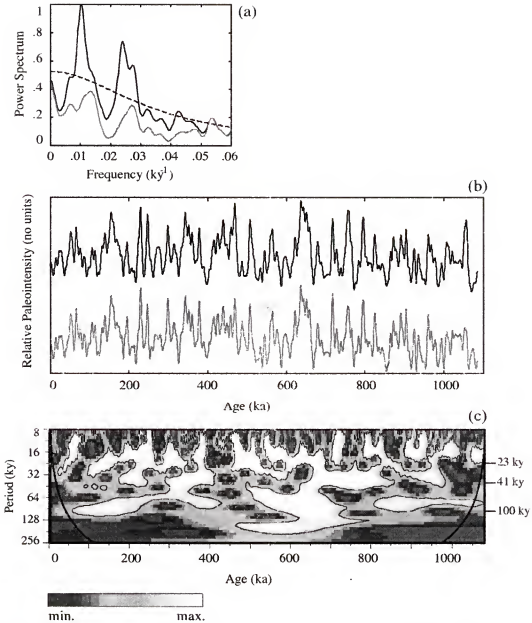


Figure 3-11. Filtering of the paleointensity record for the Fourier periods 23 kyr, 41 kyr, and 100 kyr. (a) The power spectrum of the original paleointensity record (in black) compared to that for the filtered paleointensity record (in gray) which is close to its background spectrum. (b) Comparison of the filtered (in gray) and the original (in black) paleointensity records. The filtered record was obtained by subtraction of the wavelet components at 23 kyr, 41 kyr, and 100 kyr from the initial paleointensity record. In order to facilitate the comparison, the records were slightly smoothed using a singular spectrum analysis with three principal components. (c) wavelet spectrum of the filtered paleointensity record, to be compared to the wavelet spectrum in Figure 8a.

The paleointensity record at Site 983 has been shown to be correlatable at high resolution to other paleointensity records from the Labrador sea and as far afield as the South Atlantic (Channell et al. 2000), suggesting that the lithologically-controlled secondary overprint does not strongly affect the characteristic features of the paleointensity record, and probably does not impair its usefulness for stratigraphic correlation. However, for a quantitative assessment of the level of lithologic overprint in the record, multiple records, from various lithologies and different oceans need to be compared.

CHAPTER 4

EFFECTS OF VARIABLE SEDIMENTATION RATES AND AGE ERRORS ON THE RESOLUTION OF SEDIMENTARY PALEOINTENSITY RECORDS

Introduction

Considerable information has been gathered in the past few decades on the time variations of the geomagnetic field (Dormy et al. 2000; Valet 2001). For time scales ranging from a few thousand to a million of years, most of this information has been provided by continuous records of relative geomagnetic paleointensity obtained from marine sediments (Channell et al. 1997, 1998; Channell and Kleiven 2000; Guyodo et al. 1999, 2001a; Lehman et al. 1996; Meynadier et al. 1992, 1994; Schneider and Mello 1996; Stoner et al. 1995, 2000; Tauxe and Wu 1990; Tauxe and Shackleton 1994; Tric et al. 1992; Valet and Meynadier 1993; Yamazaki et al. 1995). Those records have permitted significant progress in our understanding of the geomagnetic field behavior during polarity reversals, during geomagnetic excursions, or within periods of stable magnetic polarity (see review in Valet, 2001). The recent development of global paleointensity composites (Sint-200, Sint-800) showed that paleointensity features with wavelengths of a few tens of thousand years can be correlated worldwide (Guyodo and Valet 1996, 1999). This property of geomagnetic paleointensity has been used to develop age models in cases where the use of more traditional dating techniques is limited (Stoner et al. 1998). For shorter wavelengths, recent studies of high-resolution paleointensity records spanning the last ~ 100 ky indicate that millennial-scale correlation can be

achieved, at least regionally (Laj et al. 2000), and probably globally (Channell et al. 2000; Stoner et al. 2000). However, those high-resolution correlations are difficult to test independently, because alternative dating techniques such as oxygen isotope stratigraphy have a lower resolution than the paleointensity variations recorded in those sediments. In addition, amplitude differences are present among records with apparently correlative features, which could be lithologic in origin, but also geomagnetic in nature, as those records have sedimentation rates that should in principle allow sampling of non-dipole (local) geomagnetic intensity variations.

Over longer time-scales, comparisons of relative paleointensity records have also generated some debates. There have been questions about the existence of an asymmetrical saw-tooth pattern in paleointensity records from the Pacific and the Atlantic oceans (Meynadier et al. 1994; Valet and Meynadier 1993), or the presence of particular cycles in the geodynamo (Tauxe and Shackleton 1994; Tauxe and Hartl 1997), some of which corresponding to periods of the Earth's orbital parameters (Channell et al. 1998; Yamazaki 1999; Yokoyama and Yamazaki 2000). Various approaches have been followed in attempt to understand their origin. For instance, studies have investigated the possible presence of secondary signals in the records (Kok and Tauxe 1996; Meynadier et al. 1998; Guyodo et al. 2000), or the possible effects of the magnetization acquisition process (Meynadier and Valet 1996; Mazaud 1996). Recently, it has been proposed that aliasing of the geomagnetic signal induced by a coarse sampling of the field could explain the power spectra of some of the paleointensity records (Teanby and Gubbins 2000).

In the present chapter, I explore the effects of age inaccuracies on the power spectra of sedimentary paleointensity records characterized by unstable sedimentation rates. Using a numerical model, we simulate records with mean sedimentation rates ranging from 1 to 15 cm/ky. We investigate (1) whether sedimentation rates fluctuations and age errors are sufficient to explain the amplitude differences observed between paleointensity records, (2) to what extent individual records reflect global geomagnetic fluctuations, and (3) how much confidence should be placed in the power spectra of paleointensity records. Results presented in this chapter have been integrated in a paper submitted to *G-cube*.

Construction of the Model

We have developed a numerical model simulating the deposition, magnetization acquisition, and paleomagnetic measurement of marine sediments characterized by variable sedimentation rates. The initial geomagnetic intensity signal, or reference signal, is the same for all experiments, and consists of a 500 ky-long time series with intensity variations that are believed to represent (statistically) geomagnetic intensity changes (Constable and Parker 1988). The model is composed of four consecutive steps for each simulation: (1) conversion of the time series into a depth series, (2) acquisition of the magnetization and alteration of the magnetic signal, (3) measurement of u-channel samples, and (4) conversion to a time series using an age model.

Variable Sedimentation Rates

The first step in each simulation consists of converting the age-scale into a depth-scale using the appropriate sedimentation rate transfer function. This simulates the deposition of sediment on the sea floor, and instantaneous orientation of the magnetic

mineral grains with the geomagnetic field. In natural pelagic marine environments, sedimentation rates vary significantly from one geologic setting to another, with average values ranging from less than one to more than ten centimeters per thousand years. They are affected by several parameters including variations in paleo-productivity in the oceans, ice-sheet variability, or fluctuations of the carbonate compensation depth (dissolution). Overall, one can expect sedimentation rates for the past few million years to be variable on a glacial/interglacial time scale. A good example is provided by a study at Ocean Drilling Program (ODP) Site 983, covering the time interval 0.7-1.1 Ma (Channell and Kleiven 2000). The age model at that site was derived from the tuning of the precession cycles (20 ky) present in its $\delta^{18}\text{O}$ record to those of the ice volume model of Imbrie and Imbrie (1980). The tuning was obtained by correlating the outputs of a gaussian filter applied to both records, and centered at $0.05 \pm 0.02 \text{ ky}^{-1}$. The resulting sedimentation rates averaged $\sim 14 \text{ cm/ky}$, with values ranging from 5 to 22 cm/ky, and a standard deviation of $\sim 4 \text{ cm/ky}$ (i.e., $\sim 30\%$ of the mean sedimentation rate), with lower rates during glacials (Figure 4-1a). In this record, the typical time step separating two tie-points ranges from 5 to 10 ky. Between successive intervals, significant changes (20-30%) in sedimentation rates are common, which means that sedimentation rates probably change significantly over shorter time intervals of only a few thousand years.

We have attempted to take this variability into account in the numerical model. For each simulation, a sedimentation rates transfer function is constructed from a random time series with fixed mean (ranging 1-15 cm/ky) and standard deviation (30%), which is multiplied by a weight function favoring higher sedimentation rates during interglacial periods. An example of such sedimentation rates is shown in Figure 4-1b. In this

example, the average sedimentation rate is 14 cm/ky. Note that the range of sedimentation rate values (4-24 cm/ky) in this example is comparable to that of ODP Site 983 (5-22 cm/ky).

Post-Deposition Remanence Acquisition

The model also simulates the acquisition of a stable magnetization by the sediment. This is achieved by convolution of the initial signal with a “lock-in” function corresponding to a post-depositional remanent magnetization (pDRM) acquisition.

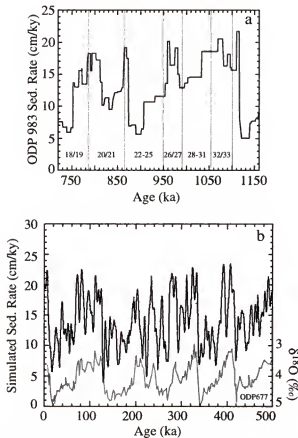


Figure 4-1. (a) Sedimentation rates calculated at ODP Site 983. The vertical lines (in gray) indicate the location of major glacial to interglacial transitions. The numbers located between the lines correspond to the oxygen isotope stages (redrawn from Channell and Kleiven (2000)). (b) Example of sedimentation rates simulated with the numerical model. ODP Site 677 benthic $\delta^{18}\text{O}$ record (Shackleton et al. 1990) is shown at the bottom, to illustrate the fact that the simulated sedimentation rates vary on a glacial/interglacial time-scale.

The actual shape and extent of the pDRM function is uncertain (Kent 1973; Verosub 1977; Hyodo 1984; Hoffman and Slade 1986; Katari et al. 2000), but it seems reasonable to assume that the lock-in of the magnetization is somewhat progressive. Magnetic grains at the top of the sedimentary column, where the water content is high and the sediment relatively unconsolidated, are able to rotate and reorient themselves along magnetic field lines. In contrast, magnetic grains located in the underlying sediment, depending on their size and shape, will be unable to rotate due to the progressive de-watering of the sediment. A simple model of pDRM consists of an exponential function (Hyodo 1984), which has been used in recent studies modeling post-depositional magnetization acquisition processes (Meynadier and Valet 1996; Mazaud 1996; Teanby and Gubbins 2000). Teanby and Gubbins (2000) also added a 8 cm uniform mixing layer (magnetization = 0) at the top of the sedimentary column, which was intended at simulating bioturbation at the sediment/water interface. However, a recent re-deposition study suggested that, at least for some lithologies, inter-granular interaction could reduce significantly the extent of pDRM, and that bioturbation may not affect the remanent magnetization below the sediment/water interface (Katari et al. 2000). The conclusions of this recent paper are in agreement with studies by Tauxe et al. (1996) and Hartl and Tauxe (1996), but contradict others (deMenocal et al. 1990; Lund and Keigwin 1994; Kent and Schneider 1995). Given the uncertainties on the matter, we chose to follow a simple approach where the pDRM function is simply given by an exponential. The parameters in this equation were selected so that 50% of the magnetization is locked within 10 cm (lock-in depth) below the sediment/water interface, and 100% within one meter.

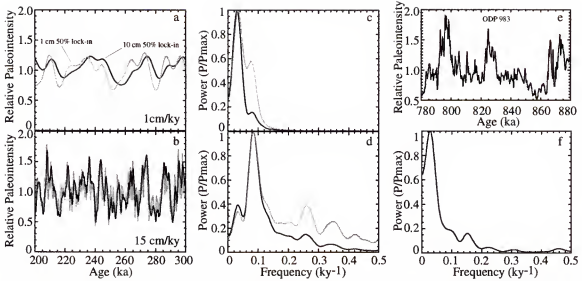


Figure 4-2. 100 ky-long relative paleointensity simulations with constant sedimentation rates of 1 cm/ky (a) and 15 cm/ky (b), and their respective power spectra (c,d). Gray curves correspond to simulations performed with a 1 cm lock-in depth, while black lines correspond to simulations done with a 15 cm/ky lock-in depth. (e) Paleointensity at ODP Site 983, for a 100 ky-long time interval of stable magnetic polarity, and associated power spectra (f).

In Figure 4-2, we have plotted the results of paleointensity simulations obtained over a 100 ky-long time interval showing sufficient variability, with lock-in depths of 1 and 10 cm, and constant sedimentation rates of 1 cm/ky and 15 cm/ky. It can be noticed that an increase in pDRM results essentially in a reduction of the amplitude of high frequencies in the paleointensity record, and that it represents an additional low-pass filter of the geomagnetic paleointensity. However, a significant fraction of the filtering is also achieved by lowering the constant sedimentation rate, as it can be deduced from the difference in resolution between the records at 15 cm/ky and 1 cm/ky. Ideally, one should be able to take a few sedimentary paleointensity records and compare their resolutions with those of the simulation. This would provide a calibration of the pDRM required in the model to fit the real data. However, as discussed in the previous section, sedimentation rates at one site are not stable over a time interval long enough to sample

the entire spectrum of geomagnetic field intensity variations. Therefore, the extent of pDRM-induced filtering in real paleointensity record would be difficult to distinguish from the one induced by sedimentation rates fluctuations. In addition, pDRM effects are probably dependant on the sediment lithology, and inter-grains interaction (Lu et al. 1990). Despite this frustrating situation, we attempted a qualitative comparison with the results from ODP Site 983, for which the sedimentation rates are well constrained. We selected the interval (780-880) ka, which corresponds to a period of stable magnetic polarity. Over this interval, the mean sedimentation rate is 15.1 cm/ky, with values ranging from 7 cm/ky to 19 cm/ky. The amplitude of the short-term oscillations appears to be lower than what was obtained in the simulation with a 1 cm lock-in depth, suggesting the presence of some pDRM-induced filtering of the signal. The presence of pDRM at Site 983 is also suggested by the shape of the paleointensity power spectra, which is closer to the one derived from the simulation with a 10 cm lock-in depth. Therefore, we chose the conservative approach and incorporated the 10 cm lock-in depth in the model.

Subsequent to the acquisition of magnetization, the model simulates the measurement of u-channel samples with a cryogenic magnetometer, with a stratigraphic step-size of 1 cm. The signal is sub-sampled at intervals of 1 cm after convolution with the response function of a u-channel magnetometer, which is a gaussian function with a half-width of about 6 cm. The top-most part of the record is subsequently removed, as the sediment is not consolidated and the magnetization acquisition only partial over this interval.

Different Age Models

In the final step of the simulation, the paleointensity records are dated using age models of variable quality. Previous studies simulating the acquisition or measurement of magnetization in marine sediments have considered constant sedimentation rates and therefore ideal dating. This situation is highly unlikely in reality, since most paleomagnetic and paleoceanographic studies report records characterized by variable sedimentation rates. For marine sediments, the most appropriate dating technique consists in correlating the oxygen isotope ($\delta^{18}\text{O}$) data at a specific site to a reference record of known age. Tie-points between the $\delta^{18}\text{O}$ record and the reference record, and the step between tie-points, will depend on the resolution of sampling and the overall quality of the isotopic record. This procedure assumes constant sedimentation rates between tie-points. If the actual sedimentation rates vary on a time scale shorter than the time step between tie-points (typically a few tens of thousand years), age offsets (of a few thousand years) are generated. In our simulations, we used four age models of variable resolution. Examples illustrating these age models are shown in Figure 4-3, where the apparent sedimentation rates resulting from the age models are compared to the actual sedimentation rates used to construct the initial depth-scale. In the first age model AM1, only two tie-points have been used. This could correspond to an age model based on magnetic polarity stratigraphy, where no isotope data are available and only the location of the magnetic polarity boundaries can be used to date the sediment. The second age model, AM2, represents a low-resolution correlation between $\delta^{18}\text{O}$ data, where only the terminations between glacial and interglacial periods have been correlated. The reference curve utilized here is the benthic $\delta^{18}\text{O}$ record of ODP Site 677 (Shackleton et al. 1990).

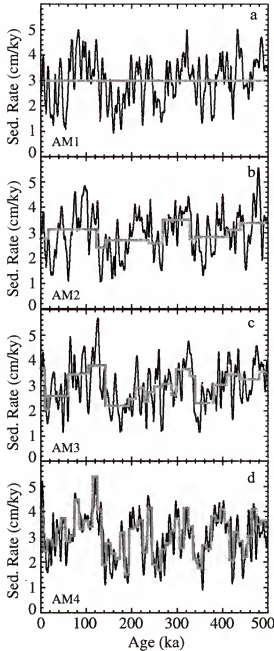


Figure 4-3. Examples of apparent (final) sedimentation rates (in gray) derived from the age models AM1 (a), AM2 (b), AM3 (c), and AM4 (d) used in the simulations, and compared to the actual (initial) sedimentation rates (in black).

The AM2 age model corresponds to an age model based on a $\delta^{18}\text{O}$ record obtained from a low-resolution sampling of the sediment, or on a $\delta^{18}\text{O}$ record that is difficult to correlate unambiguously to the reference. In the third age model AM3,

additional tie-points have been introduced. This corresponds to a medium-high resolution correlation of $\delta^{18}\text{O}$ records. The last age model, AM4, corresponds to what could be obtained with a “tuning“ of the $\delta^{18}\text{O}$ records, using the orbital precession cycles. This type of age model requires high-resolution $\delta^{18}\text{O}$ records, of excellent quality. Evidently, an age-model based on only a few tie-points will yield less variable apparent sedimentation rates, which could be wrongfully interpreted as the result of a quiet sedimentary environment (Figure 4-3).

Comparison with Real Data

In the model described in the previous section, the magnetic properties (magnetic mineralogy, grain size and shape, and concentration) and the response function of the sediment have been assumed constant throughout the entire sequence. However, natural sediments display some variations in those parameters, which influence the natural remanent magnetization (NRM) of the sediment. Ideally, paleointensity records are obtained by normalizing the NRM with a magnetic parameter reflecting variations in concentration of the grains that carry the NRM. If the normalization has been done correctly, the resulting record should display geomagnetic paleointensity changes (see review in Tauxe 1993). A compilation of 18 paleointensity records for the last 200 ky (Sint-200) (Guyodo and Valet 1996) showed that it was essentially the case, since all records covering this time interval show similar paleointensity features. However, the correlation between the records is not perfect, and some disparity exists, which accounts for the ~10% uncertainty associated with the compilation (Guyodo and Valet 1996). Those differences could be due to uncertainties in chronologies, but also to inadequacy of

the normalization procedure resulting in overprints reflecting uncompensated lithologic variability.

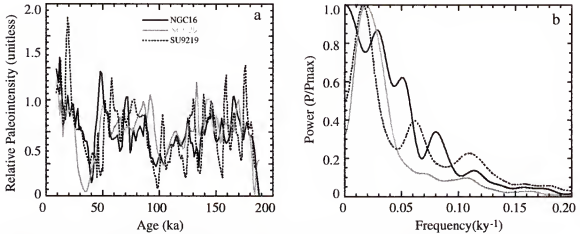


Figure 4-4. Comparison of three real paleointensity records over a 200 ky-long time interval (a), and their respective power spectra (b).

In Figure 4-4, we plot three paleointensity records of mean sedimentation rate around 3 cm/ky (Lehman et al. 1996; Yamazaki and Ioka 1994), which were extracted from the database used to construct Sint-200 (Guyodo and Valet 1996). These records have been put on a common time-scale using oxygen isotope stratigraphy, with a resolution similar to an AM3 age model (Guyodo and Valet 1996). Most of the features can be matched among the records, but they display significant differences in amplitudes. In addition, although they display the same succession of paleointensity features, their power spectra do not agree well with each other.

We tested whether or not our model could reproduce those differences. The results are shown in Figures 4-5a and 4-5b, where we have plotted the outputs of three simulations obtained with a mean sedimentation rate of 3 cm/ky for a 200 ky-long time interval. The age model of these simulations is AM3, which has a resolution similar to those of the data presented in Figure 4-4.

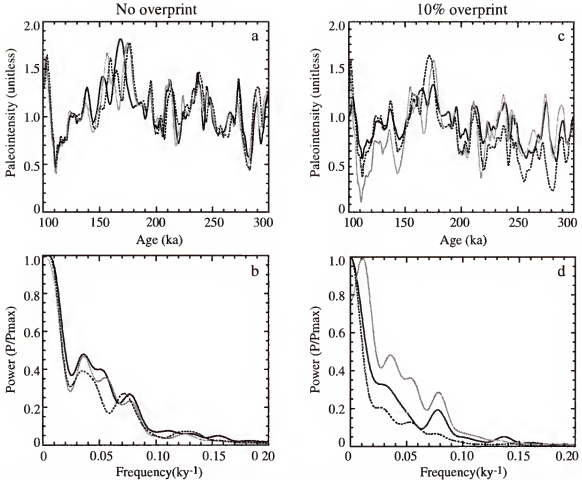


Figure 4-5. 200 ky-long simulations of paleointensity records with mean sedimentation rates of 3 cm/ky (a), and associated power spectra (b). (c) and (d) are the same as (a) and (b), with an additional 10% overprint.

Amplitude differences among the simulated records are much less marked than in the case of the real records (Figure 4-4), and the power spectra display too many similarities with respect to the real data (Figure 4-5b). This suggests that the differences in paleointensity induced by age errors are not sufficient to explain most of the differences among real records for those mean sedimentation rates. Since records characterized by mean sedimentation rates of 3 cm/ky cannot record non-dipole (local) geomagnetic intensity variations that vary on a centennial scale (Hulot and Le Mouél 1994; Hongre et al. 1998), those differences could be lithologic in nature. They have therefore to be taken into account, and a small overprint (about 10% of the standard

deviation of each paleointensity) as been added to the simulations. This secondary signal is different for each simulation, and is generated from a random iterative process with wavelengths ranging from a few centimeters to several meters. The paleointensity simulations obtained with this revised model (Figure 4-5c,d) display the same kind of differences in amplitude and power spectra as the real data (Figure 4-4), and are therefore more realistic.

Results

Individual Records

The model was used to simulate paleointensity records over a time span of about 500 ky, with mean sedimentation rates ranging from 1 to 15 cm/ky. For each mean sedimentation rate, 10 simulations were performed. The results obtained for the mean sedimentation rates of 1, 7, and 15 cm/ky are shown on Figure 4-6, over the time interval common to all the records. As could be expected, a decrease in the dispersion of the data is noticed with increasing resolution of dating (Figure 4-6). In addition, the low-resolution records seem to remain unaffected by changes in quality of the age model. For age models AM2, AM3, and AM4, there is a significant decrease in dispersion with increasing sedimentation rates. The problem inherent in the age models could be corrected if the signal was sufficiently preserved to allow positive recognition of paleointensity features among the records. This is explored in Figure 4-7a for the age model AM3. In this case, records characterized by very high mean sedimentation rates (e.g. 15 cm/ky) show features that can be uniquely correlated to dipole variations of geomagnetic field intensity, although there are some differences in amplitudes. In Figure 4-7a, relative variations of the axial dipole intensity are estimated by filtering

wavelengths shorter than 2000 years out of the reference geomagnetic signal (note that non-dipole components have time constants shorter than 150 years, and the equatorial dipole of about 500 years (Hulot and Le Mouél 1994; Hongre et al. 1998; Dormy et al. 2000)). Low amplitude geomagnetic variations of slightly smaller wavelength, possibly corresponding to the equatorial dipole, are also present in some records. Therefore, our results suggest that paleointensity records with mean sedimentation rates up to 15 cm/ky display essentially global geomagnetic time variations associated with the main axial dipole. This result tends to support previous findings which imply that paleointensity records from the North Atlantic to the South Atlantic oceans can be correlated (Channell et al. 2000; Stoner et al. 2000). Maximum offsets between the synthetic records and the reference geomagnetic variations are less than 4-5 ky (Figure 4-7a). They are sufficiently small to allow correct matching of dipole variations from one record to the other. Therefore, one could use high-resolution relative paleointensity records to develop a global geomagnetic paleointensity stratigraphy. Successive intensity dips in individual records are sometimes separated by as little as 2 ky (Figure 4-7a), which suggests that a precision of two thousand years could be achieved with paleointensity stratigraphy. One application would be to provide important information about leads and lags between paleoclimatic proxies in different regions of the globe.

Records with medium- to high-sedimentation rates (e.g. 7 cm/ky) can also be correlated to one another and to the axial dipole signal with confidence (Figure 4-7a). For low-sedimentation rates (e.g. 1 cm/ky), the identification of most of the geomagnetic features is uncertain. Essentially, only the major paleointensity dips (like the one at 310 ka) and broad trends are recorded. For those records, offsets between the records and the

reference geomagnetic intensity can be greater than 10 ky. Direct correlation with higher sedimentation rate simulations is also fairly difficult. When records characterized by different quality age models are compared (Figure 4-7b), the correlation is not easy to establish.

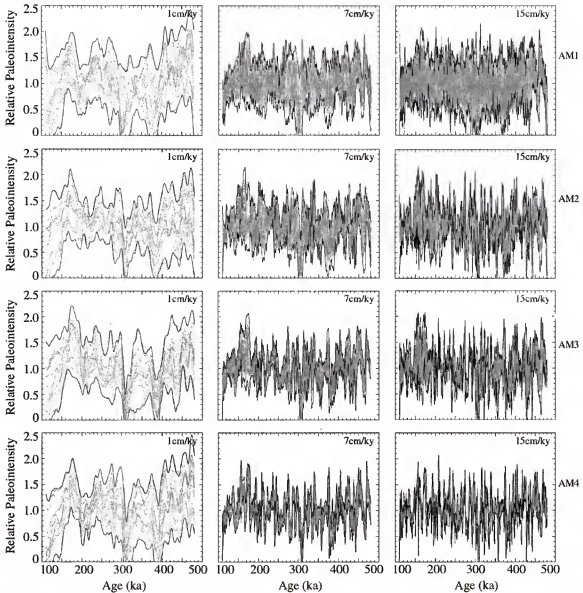


Figure 4-6. Paleointensity records simulated for mean sedimentation rates of 1, 7, and 15 cm/ky, and the age model AM3. The records are represented on their common interval (110-480 ka). The black lines represent the 2-sigma standard deviation of the distribution of paleointensities for each mean sedimentation rate.

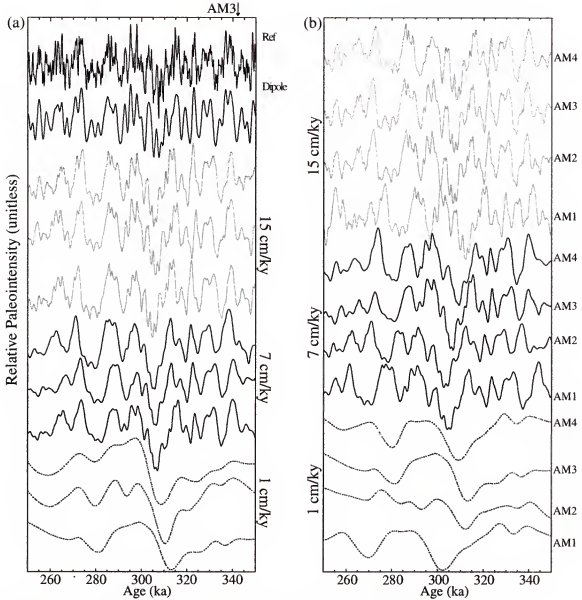


Figure 4-7. Examples of simulations. (a) Comparison of simulated records of paleointensity with the reference geomagnetic signal (at the top) from which they are derived. The age model is AM3. A “dipole” curve is also figured, which was obtained by applying a low-pass filter (> 2 ky) to the reference curve. (b) Comparison of simulated paleointensity records for different age models.

In particular, it is difficult to correlate records with drastically different mean sedimentation rates (e.g., 1 versus 7 cm/ky), and age control of variable quality. If such correlation had to be attempted, the best approach would be to inter-correlate the low-

resolution paleointensity records, and then correlate them to records of progressively increasing resolution and age control.

Individual Power Spectra

Subsequently, we investigated the effects of unstable sedimentation rates on the power spectra of individual records, for the four age models. Figure 4-8 represents the power spectra of the individual paleointensity records for mean sedimentation rates of 1, 7, and 15 cm/ky. The spectra were obtained with the Blackman-Tukey method in the software Analyseries (Paillard et al. 1996). Besides the obvious differences in the frequency range of the power spectra for different mean sedimentation rates, the power spectra vary significantly among records of similar resolution and age model. This could result in serious problems when interpreting individual power spectra in terms of geodynamo behavior. A smaller dispersion among the spectra is found for paleointensity records with high mean sedimentation rates and very good age control (AM4). In this case, most of the power spectra display a somewhat comparable succession of spectral peaks. However, they are affected by significant differences in the relative amplitudes of those spectral peaks from one record to another.

As a consequence, caution should be used when interpreting the power spectra of individual records of relative paleointensity, even when they are well dated. A more conservative and probably safer approach would be to consider either a compilation of a sufficient number of individual power spectra, or the power spectra of a compilation of paleointensity records. These methods yield average power spectra, which should reflect the spectral information common to all the records, and hopefully converge towards the power spectrum of the actual geomagnetic field.

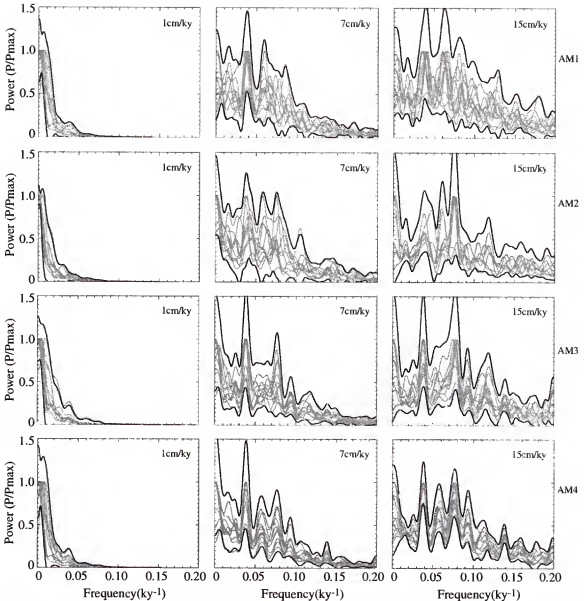


Figure 4-8. Power spectra of the records shown on Figure 4-6. The black lines represent the 2-sigma standard deviation of the distribution of power spectra for each sedimentation rate.

Stacking the Records

Compilations of the individual power spectra, as a function of mean sedimentation rate, ranging 1-15 cm/ky, are represented by color maps in Figure 4-9. Alternatively, Figure 4-10 displays the power spectra derived from stacking the 10 paleointensity records. Comparison with the reference power spectrum can be done by

visual match (Figures 4-9, 4.10), as well as by calculation of the coherence function between the compilations and the reference geomagnetic signal. Figures 4-9 and 4-10 show similar results, although the spectra are sharper (better isolation of particular spectral peaks), and the values of the coherence higher in the case of the power spectra derived from the compilation of paleointensity records (Figure 4-10). In both cases, significant differences are observed between results obtained with different age models. Naturally, compilations obtained from records dated with a low-resolution age model (e.g. AM1) incorporate records with significant age offsets, which tend to reduce the time resolution of the compilation (Figure 4-10a). For those records, there is little resemblance between the power spectra and the reference spectrum, for all sedimentation rates. For this age model, it is impossible to find any paleointensity feature of wavelength shorter than 25-50 ky that is coherent (at the 95% significance level) with those of the geomagnetic field. The coherence increases with improving age models and increasing sedimentation rates. When the age control is excellent and the mean sedimentation rate is 15 cm/ky, paleointensity features as short as 2-3 ky are coherent with the geomagnetic field at the 95% significance level. These results are summarized in Figure 4-11a, which displays the location of the 95% significance level as a function of the sedimentation rate for the four age models. Because the 95% significance level depends slightly on the power spectra, those limits have to be taken as estimates (within a few 10^{-3} ky^{-1}). AM1 is characterized by almost no variation, while there is an increase in the frequency domain of coherence with increasing sedimentation rates for the other age models. For age models AM2 and AM3, the increase is much slower than for AM4, and some “plateau”

(at ~ 10 ky for AM2 and $\sim 6-8$ ky for AM3) is reached for mean sedimentation rates higher than about 7 cm/ky.

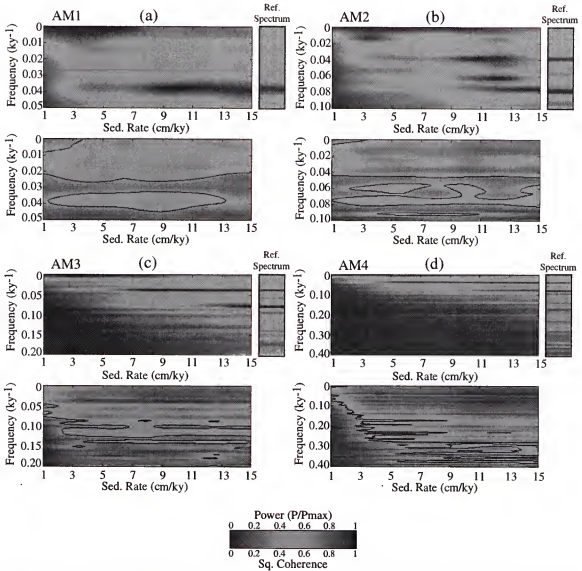


Figure 4-9. Power spectra. (a) Top: color maps of the compilation of power spectra, as a function of mean sedimentation rates ranging 1 to 15 cm/ky for the age model AM1. The power spectra can be compared to the reference spectrum (vertical color bar). Bottom: color maps of the compilation of squared coherences between the paleointensity and the reference signal, as a function of sedimentation rate, for the age model AM1. The back line corresponds to the 95% significance level. (b), (c), (d) are the same as (a) for the age models AM2, AM3, and AM4, respectively. The frequency scales vary from one subplot to the other, depending on the range of frequency where the signal is significant.

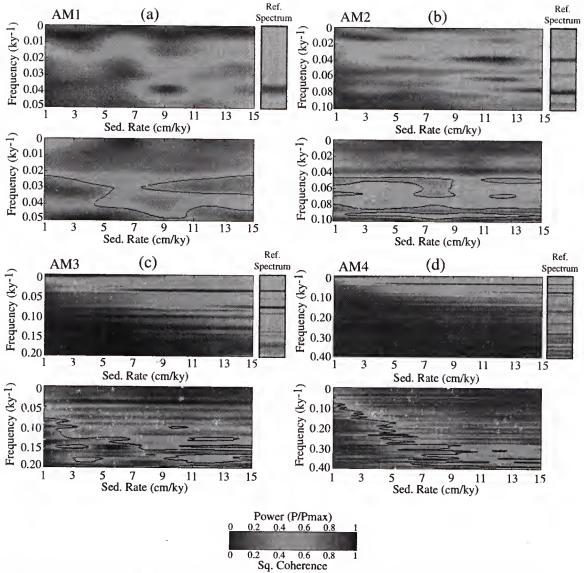


Figure 4-10. Power spectra. (a) Top: color maps of the power spectra of the stacked records, as a function of sedimentation rates ranging 1 to 15 cm/ky for the age model AM1. The power spectra can be compared to the reference spectrum (vertical color bar). Bottom: color maps of the squared coherences between the stacked paleointensity records and the reference signal, as a function of sedimentation rate, for the age model AM1. The black line corresponds to the 95% significance level. (b), (c), (d) are the same as (a) for the age models AM2, AM3, and AM4, respectively. The frequency scales vary from one subplot to the other, depending on the range of frequency where the signal is significant.

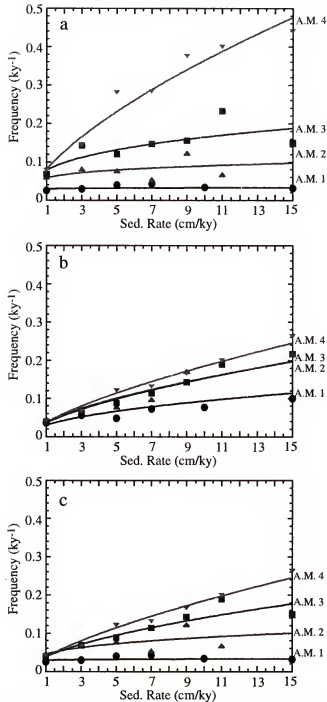


Figure 4-11. Summary of results. (a) Maximum frequency range of the coherence (at the 95% significance level) between the stacked paleointensity records and the reference signal, as a function of the sedimentation rate. (b) Limit of the 80% attenuation of the power spectra, relative to the reference spectrum. (c) Minimum value of either the frequency at which the coherence with the reference signal is lost (at the 95% level), or at which the 80% attenuation is reached.

These estimates are based on the existence of coherence between the paleointensity and the reference geomagnetic signal with values above the 95% significance level. However, the actual power in those spectral bands may be too attenuated with respect to the reference spectrum to permit the identification of any significant peaks in the paleointensity power spectrum. This point is illustrated in Figure 4-12, where we plot the power spectrum of a compilation of paleointensity records with mean sedimentation rate of 9 cm/ky (age model AM4). In this example, there is coherence between the compilation and the geomagnetic signal for frequencies up to about 0.28 ky^{-1} (i.e., wavelengths shorter than $\sim 3.5 \text{ ky}$). However, the power spectrum at that point is characterized by values that are less than 5% of the maximum value. In addition, the relative changes in amplitude for consecutive peaks in the power spectrum do not match those of the reference spectrum, and therefore would not provide reliable information on the geomagnetic field. An alternative way to examine these results is to plot the relative change in power spectrum between the original geomagnetic signal and the paleointensity stack (Figure 4-12c). It is possible to separate regions where the paleointensity power spectrum has been amplified relative to the reference spectrum, and where it has been attenuated (Figure 4-12c). The region where the correlation with the reference spectrum is unclear (Figure 4-12a) corresponds to an attenuation of the original power spectrum greater than $\sim 80\%$ (Figure 4-12c), and to a slight decrease in the coherence, although it is still above the 95% significance level (Figure 4-12b). In this example, the original (geomagnetic) spectral lines have been so altered that any interpretation would be meaningless.

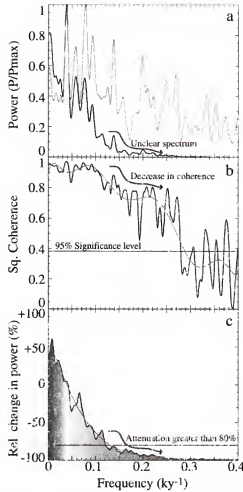


Figure 4-12. Explanation of criteria. (a) Power spectrum of a compilation of paleointensity records with a mean sedimentation rate of 9 cm/ky (in black) and the age model AM4. The power spectrum of the reference signal is represented in gray. (b) Squared coherence between the compilation and the reference signal. (c) Relative change in power between the paleointensity power spectrum and the geomagnetic reference. Positive values represent a relative amplification, and negative values a relative attenuation. The gray curves represent best polynomial fits of the data.

We used this additional criteria to re-define the maximum range of frequencies where reliable power spectra can be obtained from compilation of paleointensity records, and plotted the results in Figure 4-11b. The main observation is that values obtained for the different age models appear to be more grouped (at least AM2, AM3, and AM4) than previously, and vary almost linearly with the sedimentation rate. This result is not

surprising, since the degree of attenuation of the power spectrum should depend essentially on the degree of filtering of the original time series (i.e., the reference signal), which in first approximation is a function of the sedimentation rates. Finally, for a particular power spectrum, the maximum extent of reliability will be either the 80% spectral attenuation limit, or the 95% significance level of coherence with the reference signal, whichever is the lowest. Those values are represented in Figure 4-11c. The dependence on the age model is not as strong as in Figure 4-11a, particularly going from AM3 to AM4. Compilations of paleointensity records with low mean sedimentation rates (i.e., 1 cm/ky) provide spectral information about geomagnetic intensity variations with wavelengths larger than 25-50 ky, independent of the age-model. For higher sedimentation rates, the limit depends on the quality of the age model and on the mean sedimentation rate. A moderate mean sedimentation rate of 5 cm/ky would yield information on the dipole for time scales down to ~ 8 ky with very good age control (AM4), or down ~16 ky with a less detailed age model (AM2). For high mean sedimentation rates of 15 cm/ky, the limit is extended down from ~10 ky to ~4 ky, depending on the age model.

Conclusion

We have developed a numerical model simulating records of relative paleointensity from a reference signal containing intensity variations similar to those of the geomagnetic field. The output of our model confirms that age inaccuracies cannot explain most of the dispersion observed among existing records of similar resolution, and that some level of lithologic influence has to be considered. Comparison of records with mean sedimentation rates up to 15 cm/ky show that they all display dipole paleointensity

variations that can be traced from one record to another with confidence, provided that the difference in mean sedimentation rates does not exceed a few centimeters per thousand years. Even when the records have been dated with high-resolution correlation of $\delta^{18}\text{O}$ records, offsets of geomagnetic features between records of a few thousand years are common, which are of the same order as those observed between published paleointensity records (Stoner et al. 1998; Channell et al. 2000). Due to amplitude differences and age offsets between records, individual power spectra display significant discrepancies, which could lead to misinterpretation of some spectral peaks in term of geodynamo behavior. The accuracy of the power spectra increases when paleointensity records are stacked, and the overprints attenuated by the stacking process. Evidently, this procedure (and our model) assumes that the overprints are not coherent between sampling sites. If part of the individual overprints were a global climatic signal, the task would be more difficult. Hopefully, different sediment types and sedimentary environments will have sufficiently different lithologic influences. In any case, we recommend that compilations obtained from records at different locations and with different lithologies, should be preferred to individual records.

We compiled simulated records with mean sedimentation rates ranging from 1 to 15 cm/ky, and characterized by age models of variable quality. The power spectra obtained from those compilations reflect more or less that of the reference geomagnetic signal. However, some disparities exist between records of different sedimentation rates and age-control. When the sedimentation rates decrease, the intensity of the low-frequency variations is progressively amplified (i.e., overestimated) relative to the actual geomagnetic signal, and the high-frequency signal is attenuated (i.e. underestimated).

Independent of the age model, very low-resolution records (i.e., 1 cm/ky), provide spectral information on the field for frequencies lower than $\sim 0.02\text{--}0.04\text{ ky}^{-1}$ (25–50 ky). Therefore, their use is limited to questions regarding the general, long-term tendency of geomagnetic paleointensity. For instance, they should not be used to assess the possible influence of orbital parameters such as the obliquity (41 ky) or the precession (23 ky) on the geodynamo. A similar result is obtained for compilations derived from low-resolution age-models (e.g., those based only on magnetic polarity stratigraphy). For mean sedimentation rates higher than 1–2 cm/ky, the spectral information depends on the quality of the age-model. For instance, a compilation of records with mean sedimentation rates of 7 cm/ky can provide reliable information for time-scales as short as ~ 25 ky for a low resolution age-model, and up to ~ 7 ky in the case of a high-resolution age-model. For compilations of very-well dated sequences with mean sedimentation rates of 15 cm/ky, the power spectra provide reliable information for frequencies up to $\sim 2.5\text{ ky}^{-1}$ (~ 4 ky). At present, the only “global” compilation available to perform such spectral investigations is the Sint-800 stack, which integrates 33 records of relative paleointensity over the last 800 ky (Guyodo and Valet 1999). However, the actual resolution of the curve is rather difficult to assess, as the stack is constructed from paleointensity records with mean sedimentation rates ranging from 1 to 13 cm/ky, but is probably comparable to a mean sedimentation rate of a few centimeters per thousand years. The stack may be close to the limit of resolution necessary to firmly address questions regarding the presence of characteristic times or orbital frequencies in the geodynamo. In the present paper, we use the Blakman-Tukey spectral method, which has been employed in recent paleomagnetic and paleoceanographic studies (Channell and Kleiven 2000). Alternative, data-adaptive

methods such as wavelet analysis may provide a more efficient treatment of the problem. Nevertheless, the situation should improve with the production of new compilations of high-resolution paleointensity records, with excellent age control, and from a variety of marine environments.

CHAPTER 5

DECONVOLUTION OF U-CHANNEL PALEOMAGNETIC DATA NEAR GEOMAGNETIC REVERSALS AND SHORT EVENTS

Introduction

An increasing number of high-resolution sedimentary paleomagnetic studies have been published in the past decade, due in part to the development of pass-through cryogenic magnetometers allowing fast, automatic, and continuous measurement of sediment cores (Channell et al. 1997, 1998; Channell and Kleiven 2000; Guyodo et al. 1999, 2001a; Meynadier et al. 1992; Tauxe and Shackleton 1994; Tric et al. 1992; Schneider and Mello 1996; Stoner et al. 1995; Valet and Meynadier 1993; Yamazaki et al. 1995). These magnetometers are equipped with pick-up coil sensors permitting measurement of the magnetization along three axes, which are characterized by a response function close to a bell-shaped curve with a half-peak width of several centimeters. Due to the size of the sensor response functions, the magnetization measured at a particular position on the sediment core is integrated over a few centimeters, therefore smoothing significantly the signal. In the case of Ocean Drilling Program (ODP) piston cores, for instance, shipboard paleomagnetic measurements are performed with a resolution of ~ 7.5 cm, on 150 cm-long core sections that have been divided lengthwise into *working* and *archive* halves characterized by a cross section of about 17.1 cm^2 . A few studies have attempted to correct for this smoothing by developing deconvolution procedures aimed at increasing the spatial resolution of the data

(Constable and Parker 1991; Oda and Shibuya 1996). Alternatively, the resolution can be improved substantially by using sensors with narrower response functions, owing to a smaller diameter of the pick-up coils. This is the case with cryogenic magnetometers designed to measure u-channel samples, which are transparent plastic tubes ($2 \times 2 \times 150 \text{ cm}^3$) used to sample piston cores (Tauxe 1983; Nagy and Valet 1993; Weeks et al. 1993). However, u-channel magnetometers still provide data integrated over a few centimeters, which may pose a problem for the study of rapid geomagnetic changes such as geomagnetic excursions, which are generally recorded within only a few centimeters in sediment cores. It is therefore worth exploring whether the deconvolution of u-channel data could improve significantly their resolution over intervals characterized by rapid variations in their magnetization. For that purpose, we use the three-dimensional numerical code recently developed for ODP piston cores by Oda and Shibuya (1996), which is based on Bayesian statistics. In this scheme, the magnetization vector is modeled as a smoothly changing function, which degree of smoothness is obtained by minimizing the Akaike's Bayesian Information Criterion (ABIC). This method appears to be more stable than the one proposed by Constable and Parker (1991), which was based on a comparison between the model residuals and the observational error (Oda and Shibuya 1996). In addition, this program has a more realistic approach, as it treats the three components of magnetization (X, Y, and Z) simultaneously, and incorporates interactions between components (cross terms of the response function). The reliability of this deconvolution program was tested initially by Oda and Shibuya (1996) using shipboard ODP paleomagnetic data measured at 5-mm intervals on the archive halves of piston cores from ODP Site 769. The deconvolved data were compared with results

obtained from discrete samples extracted from the working halves of the same cores. The deconvolution procedure yielded a spatial resolution of about 2 cm, and a good agreement was found between deconvolved and discrete data (Oda and Shibuya 1996, 2000). However, the discrete samples were taken at 5-cm intervals only, such that a direct, high-resolution comparison was not performed with these samples. In the present study, we propose to test the application of the deconvolution scheme to u-channel samples that are routinely measured at the University of Florida with a spacing of one centimeter (i.e., twice the measurement spacing of the ODP cores used in the initial studies). Results of the deconvolution treatment are compared with data obtained on 1 cm-thick slices of the same u-channels. Subsequently, the deconvolution program is applied to paleomagnetic data obtained from ODP Sites 983 and 984 in the North Atlantic Ocean, which document a short geomagnetic event at about 1.255 Ma.

Response Functions

The numerical code developed by Oda and Shibuya (1996) was adapted to the type of data generated by the *2G-Enterprises* u-channel magnetometer hosted by the Department of Geological Sciences at the University of Florida. The input procedure of the initial version of the program was modified to permit uploading of data obtained with u-channel samples measured every centimeter, with a header and a trailer of 10 cm (a 1.5 m-long u-channel yields therefore 171 measurements). The procedure requires the input of a file containing the cross-section of the sample (4 cm^2) and the response function of the magnetometer sensors, with a sampling resolution similar to the one of the u-channels (Oda and Shibuya 1996). Since the u-channels are measured every centimeter, the response functions of the pick-up coils were sampled at 1 cm intervals.

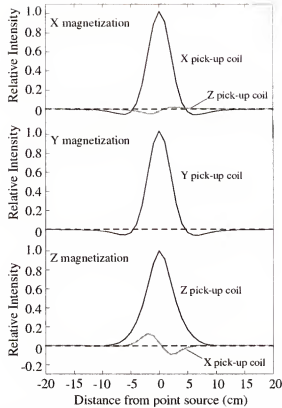


Figure 5-1. Normalized response function of the u-channel magnetometer. The solid lines represent the response of the X, Y, and Z pick-up coils when the magnetization is in the X, Y, and Z directions, respectively. The gray lines represent the response curve of the Z-axis to a magnetization oriented in the X direction (top), and of the X axis to a magnetization oriented in the Z direction (bottom).

The measurements were performed with a 4-mm-edge plastic cube containing a point source with a magnetic moment of $2.3 \times 10^{-7} \text{ Am}^2$, placed on the vertical wall of a plastic holder fixed to the sample tray of the u-channel magnetometer. A 4 cm^2 -grid was drawn on the vertical wall of the holder such that the plastic cube could be positioned at nine locations in the sensing region of the magnetometer. This permitted the measurement of the magnetometer response function in a region corresponding to the cross-section of a u-channel. The response functions of the nine locations were subsequently integrated to reflect as accurately as possible the average response of the sensors in the region occupied by the u-channel during its measurement. This procedure

accounts for possible lateral non-homogeneity of the response function of the magnetometer, in the region of measurement. The response curves were measured in the X, Y, and Z directions when the cube was oriented in X, Y, and Z, respectively, and normalized by the Z intensity peak value (Figure 5-1). The deconvolution procedure also incorporates the cross terms between the X and Z coils (Oda and Shibuya 1996). The half-peak widths of the response function are ~4.5 cm on the X and Y axes, and ~5.5 cm on the Z axis.

Deconvolution of U-channels and Comparison with Discrete Samples

We selected two u-channels among those sampled from the piston cores recovered at ODP Site 1090 in the South-Atlantic, sub-Antarctic ocean, which are characterized by a natural remanent magnetization (NRM) with significant directional and intensity variations (Shipboard Scientific Party 1999). The first u-channel sample corresponds to section 1090D-17H-1, and the second u-channel to section 1090E-22H-6. Both u-channels are 1.5 m-long and have been stepwise alternative field (AF) demagnetized with AF peak values up to 100 mT. For each demagnetization step, the NRM was measured every centimeter, with a header and a trailer of 10 cm at the beginning and at the end of the u-channel, respectively. A complete paleomagnetic study of the samples collected at site 1090 is still in progress and will be published elsewhere, such that the data reported here are limited to those only necessary for the present demonstration, and correspond to the NRM after demagnetization at 100 mT. The discrete sub-samples were extracted from the portion of the u-channels that were not part of the composite section for Site 1090.

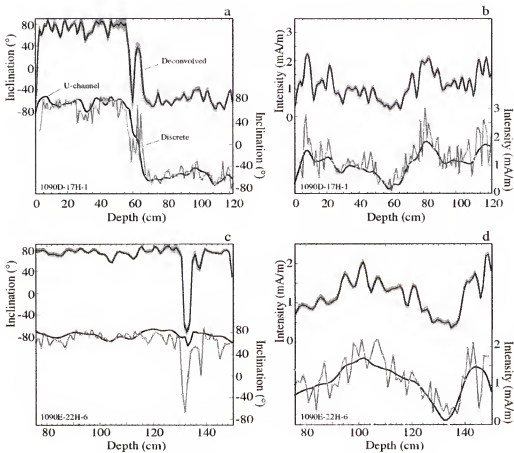


Figure 5-2. Comparison between deconvolved and discrete samples inclination (a,c) and intensity (b,d). The deconvolved data are plotted at the top of each figure. The 95% confidence interval on the deconvolution is depicted as gray shading. Open squares represent discrete data. The initial u-channel data are represented by thick lines superimposed to the discrete curves. The errors associated with the discrete measurements are smaller than the symbols used to plot the data.

The discrete sampling was performed between 0 and 122 cm for section 17H-1, and between 76 and 150 cm for section 22H-6. These samples were obtained by cutting 1 cm-thick slices of the sediment contained in the u-channels. A few discrete samples, corresponding to intervals with coarser sediment, were damaged during the sampling and were excluded from this study. The discrete samples were measured in eight orientations on the three-axis discrete magnetometer located in the paleomagnetic laboratory of the University of Florida (Figure 5-2).

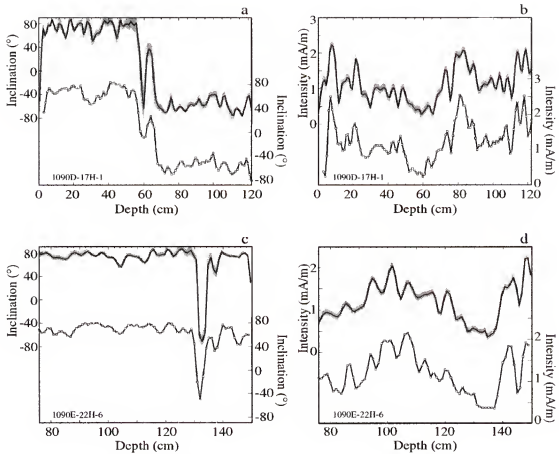


Figure 5-3. Comparison between deconvolved and discrete samples inclination (a,c) and intensity (b,d). The discrete sample data have been smoothed to slightly reduce their resolution.

The u-channels were also measured in eight orientations before deconvolution and comparison with the discrete samples. In Figure 5-2, the deconvolved u-channels inclination and intensity variations (averaging eight deconvolutions) are compared to the results obtained on the discrete samples. The most noticeable observation is that small amplitude features in the u-channel data are considerably amplified by the deconvolution. For instance, the small inclination modulation at about 60 cm in section 17H-1 corresponds to a drastic change of about 100° (from $\sim 40^\circ$ to $\sim 60^\circ$) in the deconvolved data (Figure 5-2a). Similarly, in section 22H-6, the small directional change, at about 130 cm down section, becomes after deconvolution what might be interpreted as

a short geomagnetic event (Figure 5-2c). These major changes are in good agreement with those recorded by the discrete samples, which attests to the validity of the deconvolution results over these two intervals (Figure 5-2). Overall, the deconvolved data have a lower resolution than the discrete data, and direct comparison between the two data sets is not always obvious. An alternative comparison is proposed in Figure 5-3, where the resolution of the discrete sample data has been reduced to simulate what would be obtained with 8 cm^3 discrete samples taken every 2 cm (continuous sampling), which is the standard size for discrete paleomagnetic plastic cubes. Discrete and deconvolved intensity variations are in good agreement, except for a few features of small amplitude. These differences may be the consequence of slight disturbances of the discrete samples, and/or to small stratigraphic errors of a few millimeters occurring during sub-sampling of the u-channels. Alternatively, they could be inaccuracies in the deconvolution results, possibly due to inexactitudes in the sensor response functions or to errors inherent to the method. Additional errors may emerge from small lateral displacements of the u-channels during measurements.

The Bjorn Geomagnetic Event at ODP Sites 983 and 984

We subsequently applied the deconvolution scheme to paleomagnetic data from u-channels collected from cores recovered in the North Atlantic during ODP Leg 162 at Sites 983 (60.4°N, 23.6°W) and 984 (61.4°N, 24.1°W). The high sedimentation rates at these sites, higher than 10 cm/ky, allowed the recovery of detailed paleomagnetic records spanning the last ~2 My (Channell et al. 1997, 1998; Channell 1999; Channell and Kleiven 2000).

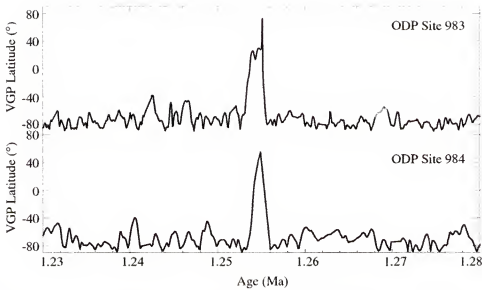


Figure 5-4. Virtual geomagnetic pole (VGP) latitude at Site 983 (top) and 984 (bottom) between 1.23 and 1.26 Ma. The Excursion at about 1.255 Ma correspond to the Bjorn event reported by Channell et al. (in press).

Recently, Channell et al. (in press) reported the presence of several geomagnetic excursions in the directional paleomagnetic record of the Matuyama Chron at these two sites. One of those, which was named the Bjorn event, appeared as a rapid change in the direction of magnetization around 1.255 Ma, below the Cobb Mountain event (Channell et al. 2001). The virtual geomagnetic pole (VGP) latitudes calculated from the component directions of the NRM (Channell et al. in press) are shown in Figure 5-4 for a time interval encompassing this event. The Bjorn event represents a good candidate for the testing of the deconvolution program, since it is recorded within only a few centimeters of sediment (less than 30 cm). It is nearly synchronous at both sites, although the shape of the excursion is somewhat different from one record to another. This is partly due to the slight difference in resolution of the two records, since Site 983 has a sedimentation rate of ~ 14 cm/ky and Site 984 is characterized by a sedimentation rate of ~ 10 cm/ky over this interval.

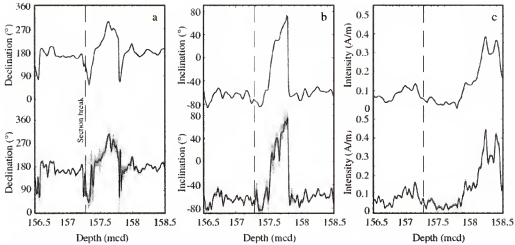


Figure 5-5. Variations of the declination (a), inclination (b), and intensity (c) of the NRM at Site 983, after alternative field demagnetization at 25 mT. Curves at the top of each sub-figure correspond to the initial u-channel data, while those at the bottom correspond to the deconvolved data. The gray shaded area are the 95% errors associate with the deconvolution treatment. The dashed lines indicate a change of core section (i.e., of u-channel).

The u-channel data corresponding to the NRM demagnetized at peak AF values ranging from 20 to 140 mT were treated with the deconvolution program over the interval encompassing the event. Figures 5-5 and 5-6 display the results of this deconvolution procedure for the NRM after AF demagnetization at 25 mT. The deconvolution appears to be more efficient for Site 984 than for Site 983, as indicated by the lower values of the errors associated with the calculation for Site 984. Nevertheless, there is an increase in the resolution of the data at both sites. In Figure 5-7, we show the component directions calculated with the standard least-square method (Kirschvink 1980) for the demagnetization interval 25-140 mT. Overall, these directions are well defined, as demonstrated by the low values of the maximum angular deviation (92% are less than 5°, and 99% are less than 10°). During the Bjorn event, there is a general agreement between the deconvolved data at the two site, which is best observed when they are plotted in term of VGP latitude versus age (Figure 5-8).

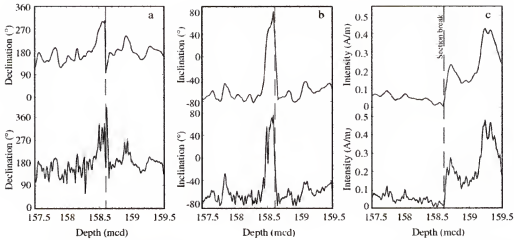


Figure 5-6. Variations of the declination (a), inclination (b), and intensity (c) of the NRM at Site 984, after alternative field demagnetization at 25 mT. Curves at the top of each sub-figure correspond to the initial u-channel data, while those at the bottom correspond to the deconvolved data. The gray shaded area are the 95% errors associate with the deconvolution calculations. The dashed lines indicate a change of core section.

At both sites, the VGP latitude record is characterized by a rapid departure from southern latitudes around 1.2555 Ma, followed by a more progressive return to the initial average position, with a “plunge” at about 1.2545 Ma. The two records appear in better agreement with each other than before the deconvolution (Figures 5-4 and 5-7).

Summary

We investigated the possibility of applying the three-dimensional deconvolution scheme proposed by Oda and Shibuya (1996) to paleomagnetic data routinely acquired on u-channel samples at intervals of one centimeter. Two u-channels characterized by drastic changes in magnetization were deconvolved and the results were compared with data obtained on discrete samples extracted at one centimeter intervals from the same u-channels. This comparison suggests that deconvolved data have a spatial resolution lower than that of the 1-cm discrete samples, but close to what would be obtained from 8 cm³ paleomagnetic cubic samples. Large amplitude changes in the intensity and direction of

the magnetization of discrete samples, during a reversal and a possible short geomagnetic event, are reproduced confidently by the deconvolved u-channel data.

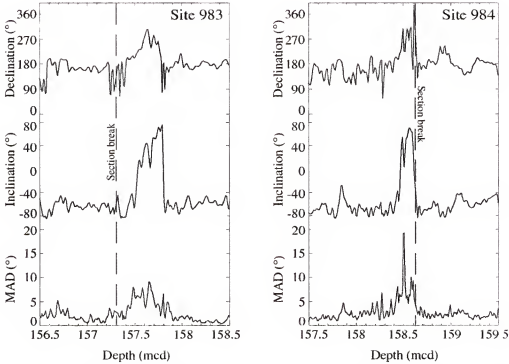


Figure 5-7. Component declination (top) and inclination (middle), and associated maximum angular deviation (MAD) values (bottom) calculated from the deconvolved data at Sites 983 (a) and 984 (b). The components were computed for the demagnetization interval 25-140 mT. The dashed lines indicate a change of core section.

The numerical code was also used to deconvolve u-channel data from ODP Sites 983 and 984 containing a short geomagnetic excursion. A significant increase in the resolution of the directional record of this event is observed at both sites, which display a better agreement among each other than before the deconvolution treatment. The duration of the Bjorn event, based on the time interval between equator crossings, is less than two thousand years.

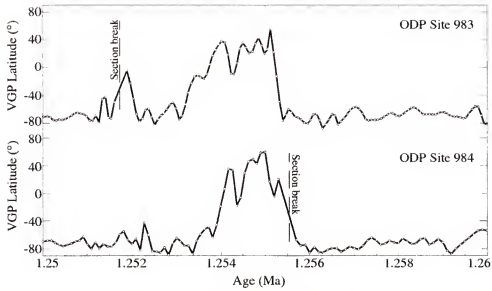


Figure 5-8. Virtual geomagnetic pole (VGP) latitude calculated from the deconvolved direction data at Site 983 (top) and 984 (bottom) around the Bjorn geomagnetic excursion.

CHAPTER 6

CONCLUSIONS AND PERSPECTIVES

The results presented in this dissertation illustrate the possibility of extracting reliable information about the geomagnetic field time variations, from the analysis of the remanent magnetization of marine sediments. The amount of information provided by a particular sedimentary record depends on multiple factors including lithologic influences, variable sedimentation rates, uncertainties in the age models, and smoothing effects induced during measurement. The use of spectral analysis techniques, such as wavelets, allows recognition and quantification of some of these influences. The construction of numerical models of magnetization acquisition permits to estimate the effects of variable sedimentation rates and dating errors. Also, the development of deconvolution schemes may favor the reduction of some of the biases introduced by the measurements.

Nevertheless, we are still far from a full understanding of the complex nature of the magnetization process. Numerous additional studies are needed, some of which requiring a cooperative effort between fundamental rock-magnetic studies and the intensive use of imaging and analytical techniques. A combination of these techniques is necessary to observe the formation and alteration of magnetic particles, and their physical and chemical interaction with the non-magnetic fraction of the sediment, or with microorganisms. With this goal in mind, I have been working on a collaborative project aimed at imaging iron-bearing particles in sedimentary rocks. The magnetization in sediments and rocks is usually carried by micron-scale grains of iron oxide or iron

sulfide. Information about the average magnetic mineralogy and magnetic grain size of geologic samples is routinely provided by rock magnetic studies. However, the origin of the magnetic grains is often unclear, and their association with the non-magnetic fraction of the sediment is usually poorly known.

In order to understand the origin and role of these particles in the magnetization process, it is crucial to examine their occurrence in their natural setting. Unfortunately, because of the scarcity and small size of these particles, in-situ detection and imaging with traditional microscopy techniques is extremely difficult. This led us to consider complementary methods such as the highly sensitive x-ray fluorescence mapping techniques available at Sectors 10 (MR-CAT) and 13 (GSECARS) of the Advanced Photon Source (APS), to locate Fe-bearing minerals present in pelagic limestone samples. The fluorescence maps are being used to study the distribution of magnetic grains, determine their composition, estimate their grain size for comparison with estimates based on magnetic parameters, and determine their relationship to the non-magnetic matrix.

The x-ray undulator beams at Sectors 10 and 13 have been used to provide area scans of thin polished sections of Cretaceous (~120 Myrs old) limestone from the Maiolica Formation (Italy) (Channell and McCabe 1994). The experimental setup used to obtain these maps is drawn in Figure 6-1. The samples are placed on a X-Y-Z stepping motor stage positioned at 45° to an incident synchrotron x-ray beam. A first detector (I_0), located between the incident beam and the sample, monitors the changes in intensity of the incoming beam. A second detector (I_f), at 45° to the sample, measures the intensity of the fluorescence coming out of the sample. In some cases, a third detector (I_t), placed

behind the sample, measures the intensity of the beam transmitted through the sample. It was not used in the limestone experiments, because the samples were too thick. Since different elements emit fluorescent x-ray photons of specific energies, it is possible to map a particular element by selecting a specific range of energies. A surface map, representing the distribution of Fe, is obtained by moving the sample in the X and Y directions relative to the incoming beam, and by measuring the ratio of the fluorescence intensity (I_f) to the incoming beam intensity (I_o). The ratio I_f/I_o is proportional to the concentration of Fe atoms in the volume hit by the x-ray beam. This experimental setup is sensitive to concentrations of one part per million or less. The size of the beam, and therefore the map resolution, can be established by two methods. A first method consists in placing a set of horizontal and vertical slits in front of the incoming beam, which define a window through which a fraction of the beam is transmitted. Beam sizes down to $\sim 50\text{ }\mu\text{m}$ can be obtained easily with this system. However, because it cuts a significant part of the initial beam, this method decreases the intensity of the beam available for investigation of the sample, and therefore reduces the efficiency of the experiment (depending on the detection level of the detectors). A second method consists in using a set of Kirkpatrick-Baez (KB) mirrors, to focus the beam down to sizes ranging 1 to $5\text{ }\mu\text{m}$ (Eng et al. 1999). Because of the high sensitivity and flexibility of this dual system, elemental maps of either small ($\sim 100\text{ }\mu\text{m}$) or large (1 mm) samples with elements at low concentrations can be obtained in a short time, relative to other techniques such as electron microprobes analysis (by an order of magnitude). It can therefore be useful for a first, rapid detection of small iron-bearing particles disseminated in a large sample. A microscope equipped with a CCD camera is also mounted on the experimental table,

which permits the recording of a video image of the region investigated, and furnishes the registration necessary to relocate this region in subsequent experiments with other equipment such as optical microscopes or scanning electron microscopes (SEM).

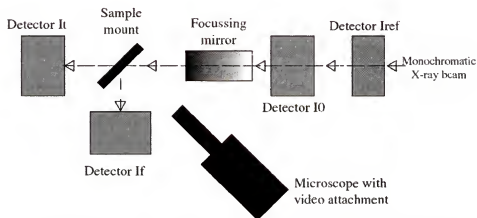


Figure 6-1. Experimental setup at Sector 10 of the APS, viewed from the top. Detectors Iref, I0, It, and If measure absorption by the reference element (Fe foil), the intensity of the incoming beam, the intensity of the transmitted beam, and the intensity of the fluorescent beam, respectively.

Discrimination of the diverse mineral phases can be determined by acquisition of micron-scale x-ray absorption fine structure spectra (XAFS) from individual grains, and comparison to standards of known composition. XAFS is an element-specific technique generally used to determine the local structure around a specific absorbing element, even when the element is at low concentration levels (Brown et al. 1988; Fendorf et al. 1994). XAFS is based on the absorption of the coherent x-rays generated by the synchrotron. A sharp increase in absorption of x-ray photons by a specific element is observed over a narrow range of incident energies (the absorption edge), which is caused by the transfer of the x-ray photons energy to the electrons of this element. At the absorption edge, the energy (which is specific to the element) is sufficient to excite an electron from a deep core state to a continuum. The photoelectron wave produced by this excitation emanates

outward from the absorbing atom. The photoelectron travels inter-atomic distances and then is backscattered by coordinating atoms. The type of neighboring atoms defines the backscattering efficiency. The backscattered wave will then encounter outgoing waves, resulting in interference effects that modifies the absorption, which produces the fine structure of the spectrum (Figure 6-2).

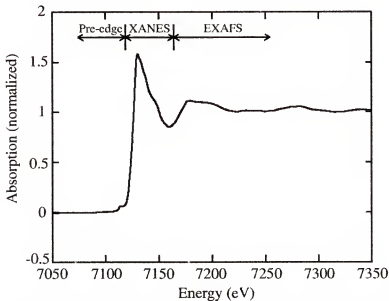


Figure 6-2. Typical XAFS spectrum for magnetite, near the iron edge energy. The ratio of I_f/I_0 is plotted as a function of the energy of the incoming x-ray beam. The normalization is obtained by assuming a step of 1 in the average absorption, for energies higher than the edge-energy.

Practically, in the fluorescence mode, a XAFS curve is obtained by reporting the ratio I_f/I_0 , for different energies around the absorption edge of a particular element (for Fe, the edge energy is 7112 eV). The spectrum is then normalized by assuming an average value of zero before the edge, and an average value of one after the edge. Three regions (pre-edge, XANES, and EXAFS) are distinguished in the XAFS spectrum. The *pre-edge* provides information about the oxidation state of the absorber, and absorber-ligand bonding. The *near edge absorption fine structure* region (XANES) is sensitive to

the arrangement of neighbors around the absorber, and can be used as a fingerprint for comparison of unknown samples to standards (Drager et al. 1988, Bajt et al. 1994, Fredrickson et al. 2000; Guyodo et al. 2001b). The *extended x-ray absorption fine structure* region (EXAFS) can be analyzed to obtain information about the distance from the absorber to near neighbors, and about the number and type of neighbors.

In our case, XANES data were collected on specific Fe-anomalies of the fluorescence maps, and were compared with spectra obtained on standards measured with the same experimental setup. The standard XANES were obtained from powders of inorganic and bacterial magnetite (Fe_3O_4), titanomagnetite ($\text{Fe}_{2.4}\text{Ti}_{0.6}\text{O}_4$), hematite ($\alpha\text{-Fe}_2\text{O}_3$), maghemite ($\gamma\text{-Fe}_2\text{O}_3$), goethite ($\alpha\text{-FeOOH}$), and pyrite (FeS_2) (Figure 6-3). The energy calibration of the beamline may fluctuate a little (of a few eV) between experiments, therefore the energies are calibrated relative to the edge energy of a standard iron foil, which XANES is acquired with another detector (Iref), synchronously to the main experiment. Subsequently, to facilitate the comparison between the data obtained on individual anomalies and those of the standards, all XANES were reported in term of relative energies, with the zero of the energy scale being the energy of the pre-edge peak of the magnetite standard. Small shifts of the edge position of particular XANES, relative to the one of magnetite, represent a relative increase (to the right) or decrease (to the left) of the oxidation state (Bajt et al. 1994). The XANES patterns obtained for magnetite, hematite, and pyrite were compatible with previously published data (Bajt et al. 1994; Drager et al. 1988). An example of an iron fluorescence map established for one of the limestone samples (AC5.46) is shown in Figure 6-4 (spot size $\sim 75\ \mu\text{m}$). Isolated regions with higher Fe content (darker spots) appear scattered over the entire surface of the

sample, suggesting a random distribution of Fe-bearing minerals in that sample. The most intense anomaly (Figure 6-4a) corresponds to a rather large ($\sim 20\ \mu\text{m}$) grain in the optical microscope image, for which a close-up is given in Figure 6-4b.

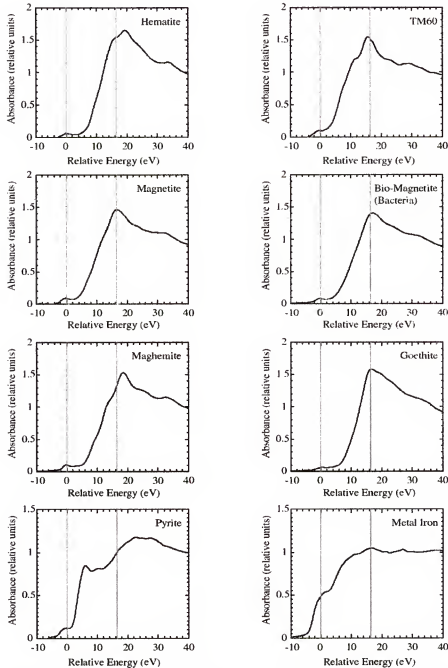


Figure 6-3. Standard XANES obtained on powders of minerals of known composition.

In Figure 6-4c is shown the XANES obtained for this anomaly, which is comparable to what was obtained with the standard FeS_2 . Confirmation of the composition was provided by energy-dispersive x-ray spectroscopy (EDX) data obtained with the scanning electron microscope (SEM) available at the university of Florida Microfabritech. The iron and sulfur EDX maps are shown in Figure 6-4d, along with the SEM image of the crystal. Another example of fluorescence maps is shown in Figure 6-5a, for a second sample (AC9.45). Again, the grains appear randomly distributed. Four Fe anomalies were selected and labeled on the map (Figure 6-5a), for which microscope images and XANES data are reported in Figure 6-5b and Figure 6-5c, respectively. The interpretation of the XANES data is not obvious, because they are probably derived from a combination of several mineral phases. The closest match was obtained with the standards of hematite and goethite, although further data analysis will be required before final identification. The larger-amplitude anomalies in the Fe map are related to larger grains. The smaller anomalies correspond to smaller grains or groups of grains, for which a more precise Fe map can be obtained with the focussed beam. An example of such maps is shown on Figure 6-6a, which corresponds to the region delimited by the small rectangle drawn in Figure 6-5a, including spots 3 and 4. In Figure 6-6a, the Fe map is compared to the optical microscope map of the same region. Small anomalies, of a few microns are present on the map (beam/step size is $\sim 5 \mu\text{m}$), which correspond to grains ranging from $\sim 10 \mu\text{m}$ to about $1 \mu\text{m}$ in size in the optical image. Three of these anomalies have been numbered in Figure 6-6a (notice that anomalies 1 and 3 correspond to Spot 3 and Spot 4 in Figure 6-5a, respectively). Close-ups of these grains are shown in Figure 6-6b.

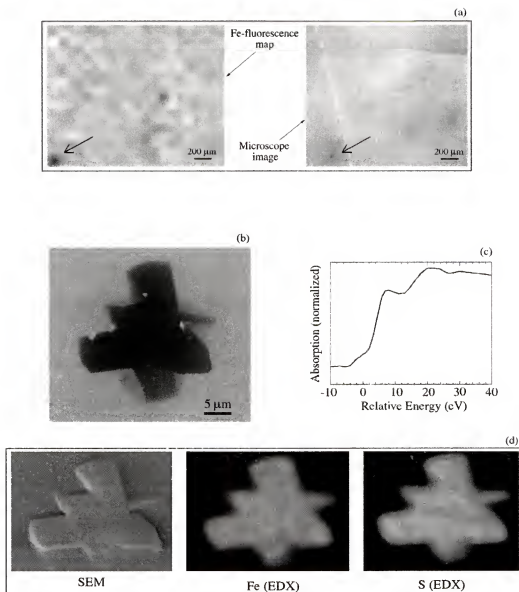


Figure 6-4. Example of fluorescence map obtained on a limestone sample (AC5.46). (a) Fluorescence map (left) and optical microscope image (right) of the sample. (b) Close-up of a grain associated with large Fe anomaly identified by an arrow in (a). (c) Normalized XANES of the same anomaly, suggesting FeS_2 as a composition. (d) Scanning electron microscope image (SEM), and energy-dispersive x-ray map (EDX) of the same grain.

Interestingly, EDX investigation of some of these grains revealed the presence of Fe-S compounds in the grains. An example is given in Figure 6-6c, for anomaly number 3. From the SEM image and the EDX elemental maps, it is possible to observe the presence of a pyrite core in the center of the grain. A likely explanation is that the grain is

derived from the partial oxidation of a pre-existing grain of pyrite. This explains also why the XANES were not uniquely correlatable to a single standard, since the grains made-up of multiple mineral phases. Other analytic techniques, such as electron microprobe or electron diffraction, are being used to further study these samples.

In any case, the methods briefly presented in this conclusion chapter provide interesting results, which, combined with other techniques of investigation, should lead to a new understanding of the composition, grain size, and distribution of Fe minerals contributing to the magnetic properties of natural sediments. The rewards of such studies will reach evidently beyond rock-magnetism and paleomagnetism, and will provide tools for domains such as the study of past environments or climates.

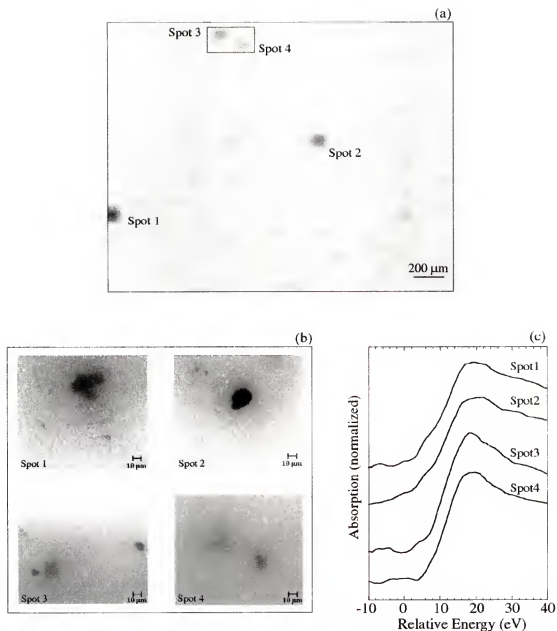


Figure 6-5. Example of fluorescence map obtained on a limestone sample (AC9.45). (a) Fluorescence map of the sample. (b) Close-up of the grains associated with 4 Fe anomalies labeled in (a). (c) Normalized XANES of the same anomalies.

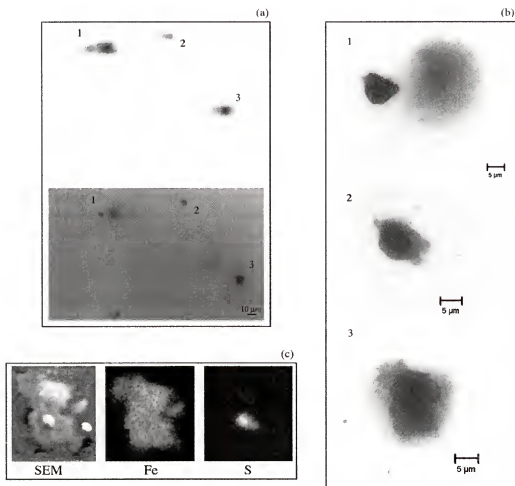


Figure 6-6. Micro-focussing fluorescence map obtained on a small region of the limestone sample (AC9.45) shown in Figure 6-5 (small rectangle). (a) Fluorescence map (top) and corresponding optical microscope image (bottom) of the region. (b) Close-up of the grains associated with 3 Fe anomalies labeled in (a). (c) Scanning electron microscope image (SEM) and energy-dispersive x-ray elemental maps of grain number 3.

LIST OF REFERENCES

- Bajt, S, S.R. Sutton, and J.S. Delaney, X-ray microprobe analysis of iron oxidation states in silicates and oxides using x-ray absorption near edge structure (XANES), *Geochim. Cosmochim. Acta*, 58, 5209-5214, 1994.
- Baumgartner, S., J. Beer, J. Masarik, G. Wagner, L. Meynadier, H.-A. Synal, Geomagnetic modulation of the ^{36}Cl flux in the GRIP ice core, Greenland, *Science*, 279, 1330-1332, 1998.
- Brachfeld, S., and S.K. Banerjee, A new high-resolution geomagnetic paleointensity record for the North American Holocene: a comparison of sedimentary and absolute intensity data, *J. Geophys. Res.*, 181, 429-441. 2000.
- Brown, GE, G. Calas, G.A. Waychunas, and J. Petiau, X-ray absorption spectroscopy: application in mineralogy and geochemistry, in FC Hawthorne (Ed.), *Spectroscopic Methods, Rev. in Min.*, 18, 431-505, 1988.
- Cande, S.C., and D.V. Kent, Revised calibration of the geomagnetic polarity timescale for the late Cretaceous and Cenozoic, *J. Geophys. Res.*, 100, 6093-6095, 1995.
- Channell, J.E.T., D.A. Hodell, and B. Lehman, Relative geomagnetic paleointensity and $\delta^{18}\text{O}$ at ODP Site 983 (Gardar Drift, North Atlantic) since 350 ka, *Earth Planet. Sci. Lett.*, 153, 103-118, 1997.
- Channell, J.E.T., D.A. Hodell, J. McManus, and B. Lehman, Orbital modulation of geomagnetic paleointensity, *Nature*, 394, 464-468, 1998.
- Channell, J.E.T., and H.F. Kleiven, Geomagnetic palaeointensities and astrochronological ages for the Matuyama-Brunhes boundary and the boundaries of the Jaramillo Subchron: palaeomagnetic and oxygen isotope records from ODP Site 983, *Phil. Trans. R. Soc. Lond. A*, 358, 1,027-1,047, 2000.
- Channell, J.E.T., A. Mazaud, P. Sullivan, S. Turner, and M.E. Raymo, Geomagnetic excursions and paleointensities in the Matuyama Chron at ODP Sites 983 and 984 (Iceland Basin), *J. Geophys. Res.*, in press.
- Channell, J.E.T. and C. McCabe, Comparison of magnetic hysteresis parameters of unremagnetized and remagnetized limestones, *J. Geophys. Res.*, 99, 4613-4623, 1994.

- Channell, J.E.T., J.S. Stoner, D.A. Hodell, and C.D. Charles, Geomagnetic paleointensity for the last 100 kyr from the sub-Antarctic South Atlantic: a tool for inter-hemispheric correlation, *Earth Planet. Sci. Lett.*, 175, 145-160, 2000.
- Constable, C., and R.L. Parker, Statistics of the geomagnetic secular variation for the past 5 Myr, *J. Geophys. Res.*, 93, 11,569-11,581, 1988.
- Constable, C., and R. Parker, Deconvolution of long-core paleomagnetic measurements: Spline therapy for the linear problem, *Geophys. J. Int.*, 104, 453-468, 1991.
- Daubechies, I., Ten Lectures on Wavelets, *Soc. Ind. Appl. Math.*, Philadelphia, Pa., 357pp, 1992.
- Day, R., M.D. Fuller, and V.A. Schmidt, Hysteresis properties of titanomagnetites: Grain size and composition dependence, *Phys. Earth Planet. Inter.*, 13, 260-266, 1977.
- DeMenocal, P.B., W.F. Ruddiman, and D.V. Kent, Depth of post-depositional remanence acquisition in deep-sea sediments: a case study of the Brunhes-Matuyama reversal and oxygen isotopic stage 19.1, *Earth Planet. Sci. Lett.*, 99, 1-13, 1990.
- Dormy, E., J.-P. Valet, and V. Courtillot, Numerical models of the geodynamo and observational constraints, *Geochem. Geophys. Geosyst.*, 1, paper number 2000GC000062[23,981 words], 2000.
- Dräger, G, R. Frahm, G Materlik, and O. Brummer, On the multipole character of the x-ray transitions in the pre-edge structure of the Fe K absorption spectra: an experimental study, *Phys. Stat. Sol.(b)*, 146, 287-294, 1988.
- Eng, P.J., M. Newville, M.L. Rivers, and S.R. Sutton, in X-ray microfocusing: applications and techniques, I. McNulty, ed., *SPIE Proc.*, 3449, 145, 1999.
- Fendorf, SE, D.L. Sparks, G.M. Lamble, and M.J. Kelley, Applications of x-ray absorption fine structure spectroscopy to soils, *Soil Sci. Soc. Am. J.*, 58, 1583-1595, 1994.
- Frank, M., Comparison of cosmogenic radionuclide production and geomagnetic field intensity over the last 200000 years, *Phil. Trans. R. Soc. Lond. A*, 358, 1089-1107, 2000.
- Frank, M., B. Schwarz, S. Baumann, P.W. Kubik, M. Suter, and A. Mangini, A 200 kyr record of cosmogenic radionuclide production rate and geomagnetic intensity field intensity from ^{10}Be in globally stacked deep-sea sediments, *Earth Planet. Sci. Lett.*, 149, 121-129, 1997.

- Fredrickson, J., J.M. Zachara, D.W. Kennedy, M.C. Duff, Y.A. Gorby, S.M. Li, and K.M. Krupka, Reduction of U(VI) in goethite (α -FeOOH) suspensions by a dissimilatory metal-reducing bacterium, *Geochim. Cosmochim. Acta*, 64, 3085-3098, 2000.
- Gauss, C.F., Allgemeine Theorie des Erdmagnetismus, *Resultate aus den Beobachtungen Magnetischen Verein im Jahre*, 1-57, 1838.
- Guyodo, Y., G.D. Acton, S. Brachfeld, and J.E.T. Channell, A sedimentary paleomagnetic record of the Matuyama Chron from the Western Antarctic margin (ODP Site 1101), *Earth Planet. Sci. Lett.*, 191, 61-74, 2001a.
- Guyodo, Y., J.E.T. Channell, M. Davidson, A. Mikhailova, H. Tostmann, M. Newville, and R. Duran, Detection and identification of Fe-bearing minerals in pelagic limestone: Micro-XANES/XAFS and fluorescence imaging, *Advanced Photon Source Activity Report*, 2001b.
- Guyodo, Y., P. Gaillot, and J.E.T. Channell, Wavelet analysis of relative geomagnetic paleointensity at ODP Site 983, *Earth Planet. Sci. Lett.*, 184, 109-123, 2000.
- Guyodo, Y., C. Richter, and J.-P. Valet, Paleointensity record from Pleistocene sediments (1.4-0 Ma) off the California Margin, *J. Geophys. Res.*, 104, 22,953-22,964, 1999.
- Guyodo, Y., and J.-P. Valet, Relative variations in geomagnetic intensity from sedimentary records: the past 200 thousand years, *Earth Planet. Sci. Lett.*, 143, 23-36, 1996.
- Guyodo, Y., and J.-P. Valet, Global changes in intensity of the Earth's magnetic field during the past 800 kyr, *Nature*, 399, 249-252, 1999.
- Hartl, P., and L. Tauxe, A precursor to the Matuyama/Brunhes transition field instability as recorded in pelagic sediments, *Earth Planet. Sci. Lett.*, 138, 121-135, 1996.
- Hoffman, K.A., and S.B. Slade, Polarity transition records and the acquisition of remanence: a cautionary note, *Geophys. Res. Lett.*, 13, 483-486, 1986.
- Hongre, L., G. Hulot, and A. Khokhlov, An Analysis of the geomagnetic field over the past 2000 years, *Phys. Earth Planet. Int.*, 106, 311-335, 1998.
- Hulot, G., and J.-L. Le Mouél, A statistical approach to the Earth's main magnetic field, *Phys. Earth Planet. Int.*, 82, 167-183, 1994.
- Hyodo, M., Possibility of reconstruction of the past geomagnetic field from homogeneous sediments, *J. Geomag. Geoelectr.*, 36, 45-62, 1984.

- Imbrie, J., and J.Z. Imbrie, Modeling the climatic response to orbital variations, *Science*, 207, 943-953, 1980.
- Jenkins, G.M., D.G. Watt, Spectral analysis and its applications, Holden-Day, 525pp, 1968.
- Katari, K., L. Tauxe, and J. King, A reassessment of post-depositional remanent magnetism: preliminary experiments with natural sediments, *Earth Planet. Sci. Lett.*, 183, 147-160, 2000.
- Kent, D., Post-depositional remanent magnetization in deep-sea sediments, *Nature*, 246, 32-34, 1973.
- Kent, D., and D. Schneider, correlation of paleointensity records in the Brunhes/Matuyama polarity transition interval, *Earth Planet. Sci. Lett.*, 129, 135-144, 1995
- King, J.W., S.K. Banerjee, and J.A. Marvin, A new rock-magnetic approach to selecting sediments for geomagnetic paleointensity studies: application to paleointensity for the last 4000 years, *J. Geophys. Res.*, 88, 5911-5921, 1983.
- Kirschvink, J.L., The least-squares line and plane and the analysis of palaeomagnetic data, *Geophys. J. R. Astron. Soc.*, 62, 699-718, 1980.
- Kok, Y., and L. Tauxe, Saw-toothed pattern of relative paleointensity records and cumulative viscous remanence, *Earth Planet. Sci. Lett.*, 137, 95-99, 1996.
- Kok, Y., and L. Tauxe, A relative geomagnetic paleointensity stack from the Ontong-Java Plateau sediments for the Matuyama, *J. Geophys. Res.*, 104, 25401-25413, 1999.
- Laj, C., C. Kissel, F. Garnier, and E. Herrero-Bervera, Relative geomagnetic field intensity and reversals for the last 1.8 My from a central equatorial Pacific core, *Geophys. Res. Lett.*, 23, 3393-3396, 1996.
- Laj, C., C. Kissel, A. Mazaud, J.E.T. Channell, and J. Beer, North Atlantic palaeointensity stack since 75 ka (NAPIS-75) and the duration of the Laschamp event, *Phil. Trans. R. Soc. Lond. A*, 358, 1009-1025, 2000.
- Lau, K.-M., H.-Y. Weng, Climate signal detection using wavelet transform: How to make a time series sing, *Bull. Amer. Meteor. Soc.*, 76, 2391-2402, 1995.
- Lehman, B., C. Laj, C. Kissel, A. Mazaud, M. Paterne, and L. Labeyrie, Relative changes of the geomagnetic field intensity during the last 280 kyear from piston cores in the Azores area, *Phys. Earth Planet. Int.*, 93, 269-284, 1996.

- Leonhardt, R., F. Heider, and A. Hayashida, Relative geomagnetic field intensity across the Jaramillo subchron in sediments from the California margin: Ocean Drilling Program Leg 167, *J. Geophys. Res.*, 104, 29133-29146, 1999.
- Lu, R., S.K. Banerjee, and J. Marvin, Effects of clay mineralogy and the electrical conductivity of water in the acquisition of depositional remanent magnetism in sediments, *J. Geophys. Res.*, 95, 4531-4538, 1990.
- Lund, S., and L. Keigwin, Measurement of the degree of smoothing in sediments paleomagnetic secular variation records: an example from late Quaternary deep-sea sediments of the Bermuda rise, western North Atlantic ocean, *Earth Planet. Sci. Lett.*, 122, 317-330, 1994.
- Mazaud, A., Sawtooth variation in magnetic intensity profiles and delayed acquisition of magnetization in deep sea cores, *Earth Planet. Sci. Lett.*, 139, 379-386, 1996.
- Meynadier, L., J.-P. Valet, F.C. Bassinot, N.J. Shackleton, and Y. Guyodo, Asymmetrical saw-tooth pattern of the geomagnetic field intensity from equatorial sediments in the Pacific and Indian Oceans, *Earth Planet. Sci. Lett.*, 126, 109-127, 1994.
- Meynadier, L., J.-P. Valet, Y. Guyodo, and C. Richter, Saw-toothed variations of relative paleointensity and cumulative viscous remanence: testing the records and the model, *J. Geophys. Res.*, 103, 7095-7105, 1998.
- Meynadier, L., and J.-P. Valet, Post-depositional realignment of magnetic grains and asymmetrical saw-toothed pattern of magnetization intensity, *Earth Planet. Sci. Lett.*, 140, 123-132, 1996.
- Meynadier, L., J.-P. Valet, R. Weeks, N.J. Shackleton, and V.L. Hagee, Relative geomagnetic intensity of the field during the last 140 ka, *Earth Planet. Sci. Lett.*, 114, 39-57, 1992.
- Morlet, J., G. Arens, E. Fourgeau, D. Girard, Wave propagation and sampling theory, 2, Sampling theory and complex waves, *Geophysic,s* 47, 203-221, 1982.
- Nagy, E.A., J.-P. Valet, New advances for paleomagnetic studies of sediment cores using U-channels, *Geophys. Res. Lett.*, 20 (1993) 671-674, 1993.
- Oda, H., and H. Shibuya, Deconvolution of long-core paleomagnetic data of Ocean Drilling Program by Akaike's Bayesian Information Criterion minimization, *J. Geophys. Res.*, 101, 2815-2834, 1996.
- Oda, H., H. Shibuya, and V. Hsu, Paleomagnetic records of the Brunhes/Matuyama polarity transition from ODP Leg 124 (Celebes and Sulu seas), *Geophys. J. Int.*, 142, 319-338, 2000.

- Paillard, D., L. Labeyrie, and P. Yiou, Macintosh program performs time-series analysis, *EOS Trans.*, 77, 379, 1996.
- Rebesco, M., R.D. Larter, P.F. Barker, A. Camerlenghi, and L.E. Vanneste, The history of sedimentation on the continental rise west of the Antarctic Peninsula, in P.F. Barker, and A.K. Cooper (Ed.), *Geology and Seismic Stratigraphy of the Antarctic Margin* (Pt. 2), Ann. Geophys. Union, *Antarctic Res. Ser.*, 71, 29-50, 1997.
- Roberts, A.P., B. Lehman, R.J. Weeks, K.L. Verosub, C. Laj, Relative paleointensity of the geomagnetic field over the last 200,000 years from ODP Sites 883 and 884, North Pacific Ocean, *Earth Planet. Sci. Lett.*, 152 (1997) 11-23.
- Sato, T., H. Kikuchi, M. Nakashizuka, M. Okada, Quaternary geomagnetic field intensity: constant periodicity or variable period? *Geophys. Res. Lett.*, 25, 2221-2224, 1998.
- Schneider, D.A., and G.A. Mello, A high-resolution marine sedimentary record of geomagnetic intensity during the Brunhes Chron, *Earth Planet. Sci. Lett.*, 144, 297-314, 1996.
- Shackleton, N.J., A. Berger, and W.R. peltier, An alternative astronomical calibration of the lower Pleistocene timescale based on ODP Site 677, *Trans. R. Soc. Edinburg Earth Sci.*, 81, 251-261, 1990.
- Shipboard Scientific Party, Site 1090, in Gersonde, R., Hodell, D.A., Blum, P., et al. Proc. Ocean Drilling Program, *Initial Reports*, 177, 1-36, 1999.
- Shipboard Scientific Party, Site 1101, in P.F. Barker, A. Camerlenghi, G.D. Acton, et al. Proc. Ocean Drilling Program, *Initial Reports*, 178, 1-83, 1999.
- Singer, B.S., M.S. Pringle, K.A. Hoffman, A. Chauvin, and R.S. Coe, Dating transitionally magnetized lavas of the late Matuyama chron: toward a new $^{40}\text{Ar}/^{39}\text{Ar}$ timescale of reversals and events, *J. Geophys. Res.* 104, 679-693, 1999.
- Stoner, J.S., J.E.T. Channell, and C. Hillaire-Marcel, Late Pleistocene relative geomagnetic paleointensity from the deep Labrador sea: regional and global correlations, *Earth Planet. Sci. Lett.*, 134, 237-252, 1995.
- Stoner, J.S., J.E.T. Channell, and C. Hillaire-Marcel, A 200 kyr geomagnetic chronostratigraphy for the Labrador Sea: Indirect correlation of the sediment record to SPECMAP, *Earth Planet. Sci. Letters*, 159, 165-181, 1998.

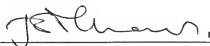
- Stoner, J.S., J.E.T. Channell, C. Hillaire-Marcel, and C. Kissel, Geomagnetic paleointensity and environmental record from Labrador Sea core MD95-2024: global marine sediment and ice core chronostratigraphy for the last 110 kyr, *Earth Planet. Sci. Lett.*, *183*, 161-177, 2000.
- Tauxe, L., Sedimentary records of relative paleointensity of the geomagnetic field: theory and practice, *Rev. Geophys.*, *31*, 319-354, 1993.
- Tauxe, L., and P. Hartl, 11 million years of Oligocene geomagnetic field behaviour, *Geophys. J. Int.*, *128*, 217-229, 1997.
- Tauxe, L., T. Herbert, N. Shackleton, and Y. Kok, Astronomical calibration of the Matuyama-Brunhes boundary: Consequences for magnetic remanence acquisition in marine carbonates and the Asian loess sequences, *Earth Planet. Sci. Lett.*, *140*, 133-146, 1996.
- Tauxe, L., and N.J. Shackleton, Relative paleointensity records from the Ontong-Java plateau, *Geophys. J. Int.*, *117*, 769-782, 1994.
- Tauxe, L., and G. Wu, Normalized remanence in sediments of the Western Equatorial Pacific, relative paleointensity of the geomagnetic field?, *J. Geophys. Res.*, *95*, 12,337-12,350, 1990.
- Teanby, N., and D. Gubbins, The effect of aliasing and lock-in processes on paleosecular variation records from sediments, *Geophys. J. Int.*, *142*, 563-570, 2000.
- Tomlinson, J.S., C.J. Pudsey, R.A. Livermore, R.D. Larter, P.F. Barker, Long-range side scan sonar (GLORIA) survey of the Antarctic Peninsula Pacific Margin, in Y. Yoshida, K. Kaminuma, and K. Shiraishi (Ed.), Recent Progress in Antarctic Earth Science, *Terra Sci. Publ.*, Tokyo, 423-429, 1992.
- Torrence, C., G. Compo, A practical guide to wavelet analysis, *Bull. Amer. Meteor. Soc.*, *79*, 61-78, 1998.
- Tric, E., J.-P. Valet, P. Tucholka, M. Paterne, L. Labeyrie, F. Guichard, L. Tauxe, and M. Fontugne, Paleointensity of the geomagnetic field for the last 80,000 years, *J. Geophys. Res.*, *97*, 9,337-9,351, 1992.
- Valet, J.-P., Time variations in geomagnetic intensity, *Rev. Geophys.*, (in review), 2001.
- Valet, J.-P., and L. Meynadier, Geomagnetic field intensity and reversals during the past four million years, *Nature*, *366*, 234-238, 1993.
- Verosub, K., Depositional and post-depositional processes in the magnetization of sediments, *Rev. Geophys. Space Phys.*, *15*, 129-143, 1977.

- Verosub, K., E. Herrero-Bervera, A.P. Roberts, Relative geomagnetic paleointensity across the Jaramillo subchron and the Matuyama/Brunhes boundary, *Geophys. Res. Lett.*, 23, 467-470, 1996.
- Weeks, R., C. Laj, L. Endignoux, M. Fuller, A. Roberts, and R. Manganne, E. Blanchard, W. Goree, Improvements in long-core measurement techniques: applications in palaeomagnetism and palaeoceanography, *Geophys. J. Int.*, 114, 651-662, 1993.
- Yamazaki, T., Relative paleointensity of the geomagnetic field during the Brunhes Chron recorded in the North Pacific deep-sea sediment cores: orbital influence? *Earth Planet. Sci. Lett.*, 169, 23-35, 1999.
- Yamazaki, T., and N. Ioka, Long-term secular variation of the geomagnetic field during the last 200 kyr recorded in sediment cores from the Western Equatorial Pacific, *Earth Planet. Sci. Lett.*, 128, 527-544, 1994.
- Yamazaki, T., N. Ioka, and N. Eguchi, Relative paleointensity of the geomagnetic field during the Brunhes Chron, *Earth Planet. Sci. Lett.*, 136, 525-540, 1995.
- Yokoyama, Y., and T. Yamazaki, Geomagnetic paleointensity variation with a 100 kyr quasi-period, *Earth Planet. Sci. Lett.*, 181, 7-14, 2000.

BIOGRAPHICAL SKETCH

Yohan J.B. Guyodo was born in Longumeau, France, and was raised in Sainte-Genevieve-des-bois, near Paris. At a young age, Yohan developed a fascination for the world of science. By the age of eleven, he had already decided to work toward a scientific career, although he had no clue about the real life of a research scientist. He attended several public schools, and obtained a high-school degree in Mathematics and Physics at the *Lycee* Albert Einstein, in Sainte-Genevieve-des-bois. He then attended the University of Paris XI, in Orsay (France) from where he graduated with a Bachelor of Science degree in Physics. Yohan received a Master of Science degree in Geophysics from the University of Paris VII. After his graduation, Yohan was employed as a paleomagnetist by the Institute de Physique du Globe de Paris, until he was incorporated by the French Air Force for one year of military service in their general headquarters in Paris. A year later, he moved to Florida for his doctoral education. During his stay at the University of Florida, Yohan was awarded a Gerson dissertation fellowship, two outstanding academic achievement awards from the College of Liberal Arts and Sciences, and an outstanding student paper award from the American Geophysical Union. Yohan is a member of the American Geophysical Union, Sigma Gamma Epsilon, and Sigma Xi.

I certify that I have read this study and that in my opinion it conforms to acceptable standards of scholarly presentation and is fully adequate, in scope and quality, as a thesis for the degree of Doctor of Philosophy.



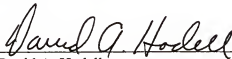
James E.T. Channell, Chairman
Professor of Geological Sciences

I certify that I have read this study and that in my opinion it conforms to acceptable standards of scholarly presentation and is fully adequate, in scope and quality, as a thesis for the degree of Doctor of Philosophy.



Neil D. Opdyke
Distinguished Professor of Geological
Sciences

I certify that I have read this study and that in my opinion it conforms to acceptable standards of scholarly presentation and is fully adequate, in scope and quality, as a thesis for the degree of Doctor of Philosophy.



David A. Hodell
Professor of Geological Sciences

I certify that I have read this study and that in my opinion it conforms to acceptable standards of scholarly presentation and is fully adequate, in scope and quality, as a thesis for the degree of Doctor of Philosophy.



Jean-Pierre Valet
Professor of Geological Sciences
Institut de Physique du Globe de Paris

I certify that I have read this study and that in my opinion it conforms to acceptable standards of scholarly presentation and is fully adequate, in scope and quality, as a thesis for the degree of Doctor of Philosophy.

A handwritten signature in black ink, appearing to read 'S. F. Dermott', written over a horizontal line.

Stanley F. Dermott
Professor of Astronomy

This dissertation was submitted to the Graduate Faculty of the Department of Geological Sciences in the College of Liberal Arts and Sciences and to the Graduate School and was accepted as partial fulfillment of the requirements for the degree of Doctor of Philosophy.

May, 2002

Dean, Graduate School